FEATURE ARTICLE

Photophysical, Photochemical and Photocatalytic Aspects of Metal Nanoparticles

Prashant V. Kamat†

Notre Dame Radiation Laboratory, Notre Dame, Indiana 46556-0579

Received: April 8, 2002; In Final Form: June 4, 2002

Unique electronic and chemical properties of metal nanoparticles have drawn the attention of chemists, physicists, biologists, and engineers who wish to use them for the development of new generation nanodevices. Metal nanoparticles such as gold and silver show noticeable photoactivity under UV−visible irradiation as is evident from the photoinduced fusion and fragmentation processes. Binding a photoactive molecule (e.g., pyrene) to metal nanoparticle enhances the photochemical activity and renders the organic−inorganic hybrid nanoassemblies suitable for light-harvesting and optoelectronic applications. The nature of charge-transfer interaction of fluorophore with gold surface dictates the pathways with which the excited-state deactivates. Obtaining insight into energy and electron-transfer processes is important to improve the charge separation efficiencies in metal−fluorophore nanoassemblies and photocatalytic activity of metal−semiconductor composites.

I. Introduction

Semiconductor and noble metal nanoclusters in the nanometer size regime display many interesting optical, electronic, and chemical properties that are size-dependent (see, for example, refs 1−13). Such nanoscale materials have potential applications in developing biological nanosensors and optoelectronic nanodevices.[12,14−18] A burst of research activity is seen in recent years in the area of synthesis and organic functionalization of different size and shape of metal nanoparticles. The size- and shape-dependent optical and electronic properties of metal nanoparticles make an interesting case for photochemists and photobiologists to exploit their role in light-induced chemical reactions.

Noble metals in bulk are photoactive only to a small extent as in the case of photoemission of electrons at silver electrodes.[19] The nanoparticles of noble metals, on the other hand, exhibit increased photochemical activity because of their high surface/volume ratio and unusual electronic properties. For example, Henglein and co-workers[20,21] reported photochemical dissolution of Ag colloids when photoejected electrons were scavenged away by species such as N_2O. The photochemical activity of metal nanocluster systems can be visualized under three different scenarios (Scheme 1). These include (i) direct excitation of the metal nanoparticles, (ii) indirect excitation achieved via surface bound fluorophore or a dye molecule, and (iii) assisting photocatalytic processes by promoting interfacial charge transfer in semiconductor−metal nanocomposites. Basic understanding of the optical properties of metal colloids, morphological changes under light irradiation, and excited-state interaction with photoactive molecules are also important for developing nanoassemblies for light-energy-harvesting and optoelectronic applications.

† Email: pkamat@nd.edu; http://www.nd.edu/~pkamat.

II. Tailored Synthesis of Nanoparticles

Several approaches have been considered to synthesize nanoparticles of transition metals in aqueous as well as nonaqueous media by adopting chemical, sonolytic, radiolytic, and photolytic reactions. (See, for example, refs 3, 7, 8, and 22−32.) Nanoparticles of Au, Ag, Pt, and Ir in toluene can be readily synthesized using a biphasic reduction procedure.[33−39] A noble metal salt (e.g., $HAuCl_4$) dissolved in water is first extracted into an organic phase containing a phase transfer reagent, tetraoctylammonium bromide (TOAB). Upon reduction with $NaBH_4$, it is possible to obtain fairly uniform size metal nanoparticles of diameter 5−10 nm. This method of preparing metal colloids in organic solvents is useful for suspending metal nanoparticles in a wide variety of solvents without allowing aggregation[40] and assembling them as two- and three-dimensional array on electrode surfaces.[41]

By employing alkane thiol as the surface capping agent one can synthesize particles as small as 2 nm in diameter. Furthermore, it is possible to control the size (particle diameter 2−30 nm) of the particle by varying the [Au]/[alkanethiol] ratio during the reduction step.[42] Using surfactant molecules in solution as template it has been possible to synthesize gold nanorods.[43−47] Irradiation of silver colloids with light (350−700 nm) results in the conversion of silver nanospheres into triangular nanoprisms.[48] This photomediated route has enabled researchers to modulate optical properties of silver nanoparticles that directly relate to the shape control. Laser irradiation also yields linear array of gold nanoparticles on gold single-crystal surfaces.[49] A surface-induced photoreaction of 4-nitrobenzenethiol has been successfully used to pattern organic monolayers on silver surfaces.[50]

Attempts to extend the chemical functionalization concept to gold nanoparticles in aqueous and nonaqueous media have

10.1021/jp0209289 CCC: $22.00
Published on Web 07/18/2002

SCHEME 1: Photochemical Activity of Metal Nanoparticles

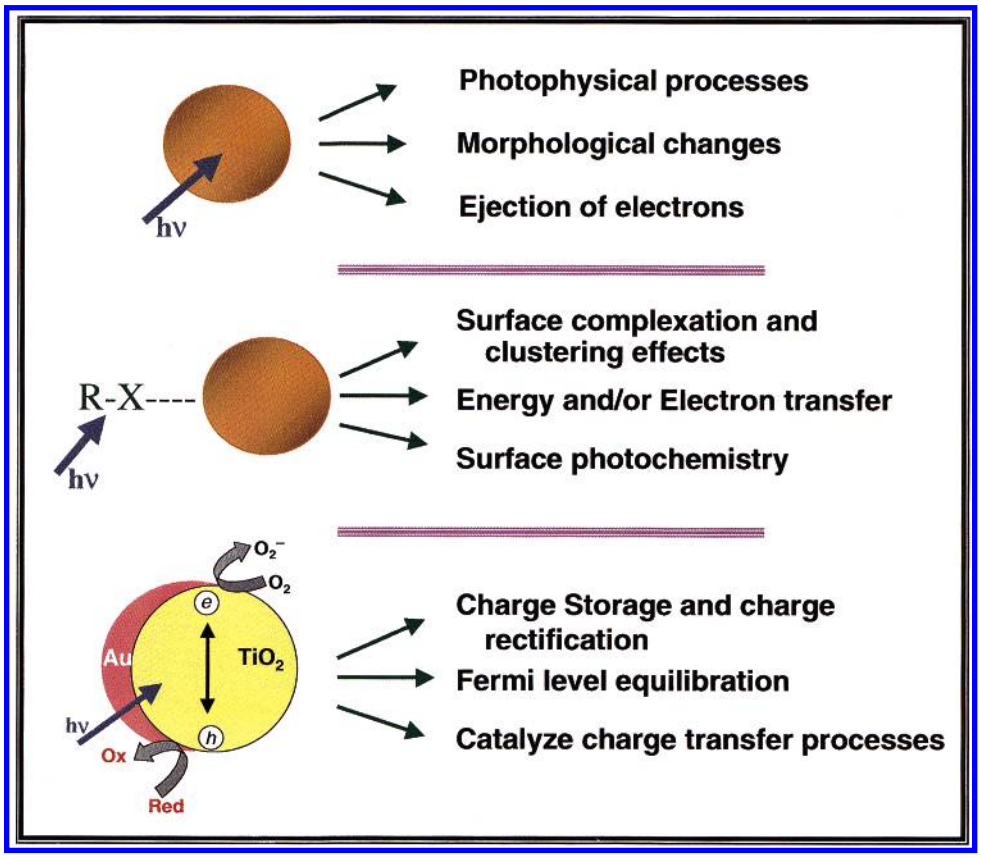

SCHEME 2: Functionalization of Gold Nanoparticles with Organic Molecules

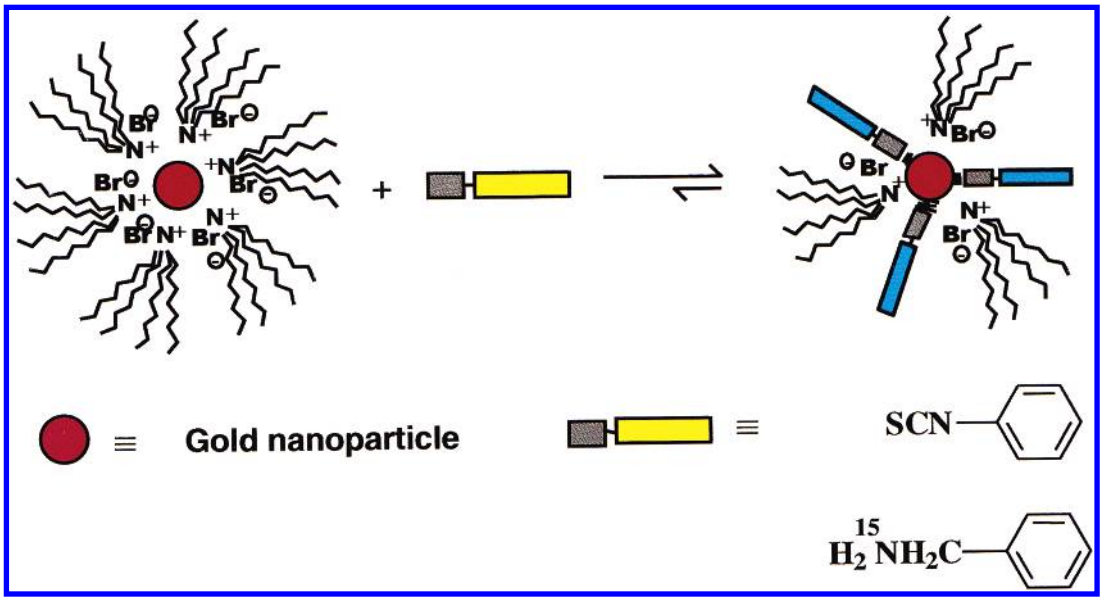

often encountered stability problems. Surface charge neutralization, which accompanies the binding of a thio or amine group to gold nanoparticles, induces aggregation and shifts the plasmon absorption to the infrared.[51−54] Photoactive molecules if chemically bound via a functional end group, such as amine, thiol, isothiocyanate, or silane, can serve the dual purpose of particle stabilization and surface modification (Scheme 2). Although most published reports focus on the synthesis of organic-capped gold nanoparticles, limited effort has been made to understand the mode of interaction of metal nanoparticles with organic capping agents and solvents.

Figure 1 shows the transmission electron micrograph of TOAB-capped and phenylisothiocyanate (PITC)-capped gold nanoparticles as deposited on carbon grids. Although the presence of TOAB capping prevents the gold nanoparticles from aggregation in solution, it is evident from Figure 1A that these particles tend to cluster upon evaporation of the solvent. On the other hand, isothiocyanate (or thiol) linkage between the gold surface and aromatic moiety produces well-ordered 2-D structures. The particles are well-separated by a uniform distance of ∼2 nm (Figure 1B). This demonstrates the feasibility of achieving desired inter particle distance by controlling the nature

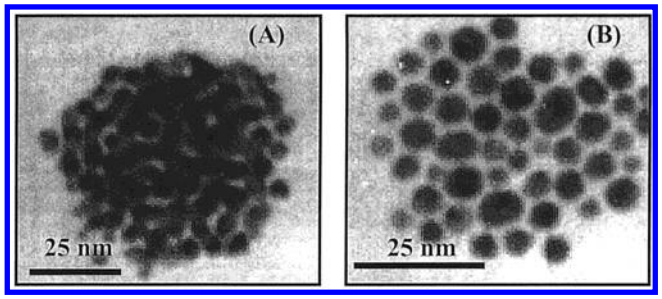

Figure 1. Transmission electron micrograph of TOAB-capped Au nanoparticles (A) before complexing with PITC and (B) after complexing with PITC. (Reprinted with permission from ref 40. Copyright American Chemical Society).

as well as size of the alkyl/aryl groups in the capping agent. Self-assembled approach of designing ordered arrays has also been attempted for other noble metals.[55−58] Other techniques such as electrophoresis and Langmuir−Blodget have also been found useful to assemble metal nanoparticles as 2-D and 3-D arrays on electrode surfaces.[59−61]

Nuclear magnetic resonance (NMR),[40,58,62−64] surface-enhanced Raman scattering (SERS),[65,66] and surface-enhanced infrared absorption (SEIRAS)[67−69] spectroscopies are two useful techniques to probe the surface-induced structural distortion of the molecular geometry and nanoparticle−molecule bonding site and binding strength. Although the SERS effect on rough noble metal surfaces was established long ago, the role of nanostructures and their specific configurations have been realized only recently. (See, for example, refs 65, 66, and 70−73). An enhancement factor of $10^{14}-10^{15}$ has been achieved enabling detection of single molecules with greater sensitivity than for luminescence. In a recent study it has been shown that single molecule SERS occurs at the junction of two aggregated particles.[74] Both the plasmon resonance of the metal nanoparticles and chemical interaction between the particle and the molecule are important for attaining the SERS activity. Correlations between transmission electron microscopy (TEM)-defined structure, ultraviolet (UV)-vis spectra, SERS signal strength, and electromagnetic theory show that the SERS signal in gold-capped silica shell arises from both the local enhancement of the dielectric field via the plasmon resonance of the nanostructure and the localized regions of high field intensity provided by the nearly completed gold shell.[75]

III. Surface Plasmon Absorption of Functionalized Gold Nanoparticles

Some similarities between metal and semiconductor nanoclusters can be drawn with respect to their physical properties.[76] They are optically transparent and act as dipoles. While conduction and valence bands of semiconductors are separated by a well-defined band gap, metal nanoclusters have close lying bands and electrons move quite freely (Scheme 3). The potential applications of these systems are mainly associated with the unusual dependence of the optical and electronic properties on the particle size.[3,7,10,11,15,26,76−82] For example, small gold nanoparticles of <5 nm diameter do not show any plasmon absorption, but gold nanoparticles of 5−50 nm show a sharp absorption band in the 520−530 nm region.[8,26] As the particles grow bigger, the absorption band broadens and covers the visible range.[15,79,83]

The metal particles of silver, gold and copper show distinct and well-defined plasmon absorption in the visible region. The surface plasmon absorption in the metal nanoparticles arises from the collective oscillations of the free conduction band electrons that are induced by the incident electromagnetic radiation. Such resonances are seen when the wavelength of the incident light far exceeds the particle diameter. In the case of silver nanoparticles, a shift in the plasmon absorption band from 400 to 670 nm is seen as the particle shape changed from spherical to triangular prisms during visible light irradiation.[48] This photoinduced transformation resulted in the color change of the colloidal suspension from yellow to green color.

Two distinct plasmon absorption bands were observed for metal nanorods corresponding to transverse and longitudinal plasmon resonance. For example, gold nanorods having an aspect ratio of 3.3 exhibit two plasmon absorption bands at 525 and 740 nm. A linear relationship between the longitudinal plasmon absorption maximum and the mean aspect ratio has been established using experimental and theoretical approaches.[84] Organization of the surfactant molecules around the gold nanorods also influence the longitudinal plasmon absorption band because of its sensitivity toward the changes in the dielectric of the surrounding medium.

The plasmon absorption of metal nanoparticles is sensitive to the surrounding environment. We can classify solvent effect into two general categories: (i) solvents that alter the refractive index surrounding gold nanoparticle and (ii) solvents that complex with the gold surface. Solvents such as cyclohexane, toluene, *o*-xylene, chlorobenzene, and *o*-dichlorobenzene do not possess any active functional groups and remain inert, with no noticeable chemical interactions, to the gold surface. The surface plasmon band of TOAB-capped Au nanoparticles in these solvents gradually shifts toward longer wavelengths with increasing refractive index of the solvent. The normalized absorption spectra of Au nanoparticles in cyclohexane and *o*-dichloromethane are shown in Figure 2. A bathochromic shift of ~10 nm was observed for TOAB-capped gold nanoparticles by varying the solvent refractive index.

The position of the plasmon absorption band can be discussed within the framework of Drude model.[85] According to Drude

SCHEME 3: Energy Levels in Semiconductor and Metal Particles

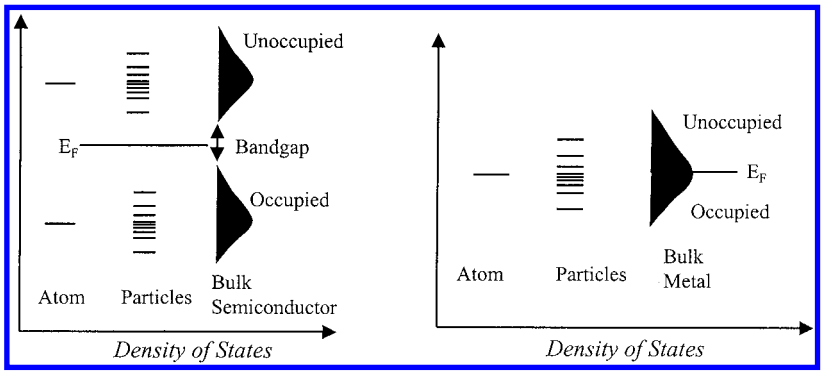

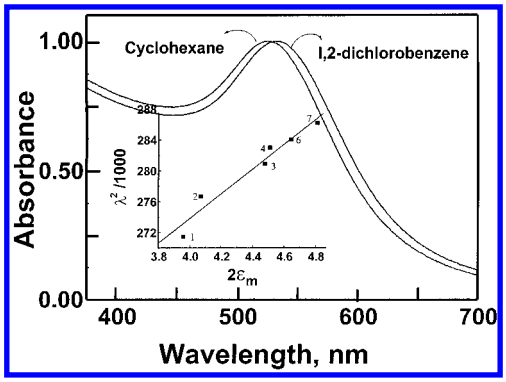

Figure 2. Normalized surface plasmon absorption band of gold nanoparticles in cyclohexane and *o*-dichloromethane. Inset shows the dependence of the square of the observed peak position of the surface plasmon band as a function of twice the medium dielectric function. (ϵ_m was determined from the expression, $\epsilon_m = n^2$) (Reprinted with permission from ref 40. Copyright 2002 American Chemical Society.)

model, the surface plasmon peak position for a spherical particle depends on the refractive index of the surrounding medium.[78,86]

$$\lambda^2 = \lambda_p{}^2(\epsilon^\infty + 2\epsilon_m) \quad (1)$$

where λ_p is the bulk plasma wavelength, ϵ^∞ is the high-frequency dielectric constant due to interband and core transitions, and ϵ_m is the medium dielectric constant. Note that the refractive index of the medium is directly related to its dielectric constant ($n = (\epsilon_m)^{1/2}$), and we can extract the information about the bulk plasmon frequency from the plot of λ^2 versus $2\epsilon_m$ from expression 1.

Plot of the square of the observed position of the surface plasmon bands of Au nanoparticles, in different solvents, as a function of twice the medium dielectric function is shown in the inset of Figure 2. A linear plot observed in this example, shows that the refractive index of the medium influences the surface plasmon maximum as per eq 1. Similar behavior of solvent dielectric dependence of plasmon absorption of gold nanoparticles[87] as well as silver and lead particles has been demonstrated in independent studies.[88] In their investigation on the effect of surface plasmon absorption of Au nanoparticle stabilized with a *comb* polymer, Underwood and Mulvaney[87] observed a 10 nm shift in the surface plasmon absorption of gold nanoparticles, when solvent refractive index was varied from $n_d{}^{20} = 1.3750$ (hexane) to $n_d{}^{20} = 1.5010$ (benzene). In contrast, Murray and co-workers[42] reported that the surface plasmon absorption of alkanethiolate-protected clusters remains almost unchanged and concluded that the Au cluster dielectric environment are more influenced by the optical dielectric of the organic ligand shell, rather than the bulk solvent.

In another recent study, Murray and co-workers[89] have modified the eq 1 to include the contribution of dielectric of the organic shell (eq 2).

$$\lambda^2 = \lambda_p{}^2[(\epsilon^\infty + 2\epsilon_m) - 2g(\epsilon_m - \epsilon_s)/3] \quad (2)$$

where g is the volume fraction of the shell layer which increases with chain length of the organic capping agent and ϵ_s is the dielectric constant of the shell. For very small gold nanoparticles (<10 nm diameter), the size of core and organic shell becomes comparable, and this in turn reduces the sensitivity of the gold plasmon absorption to the changes in the solvent refractive index. The contribution of g value becomes smaller as particle size becomes larger.

The surface plasmon absorption maximum of gold nanoparticles in solvents such as tetrahydofuran (THF), dimethylformamide (DMF), dimethyl sulfoxide (DMSO), and acetone ($\lambda_{max} = 521$ nm) remains unchanged. These polar solvents (viz., THF, DMF, DMSO, and acetone) are capable of complexing with Au surfaces through direct interaction. Stable colloids of Pd, Pt, and Au have also been prepared in polar solvents such as acetone, ethanol, 2-propanol, DMF, DMSO, or THF.[90] Small metal particles, especially gold, have high electron affinity and can strip off electrons from such solvent molecules.[91] These charged particles are stabilized by the solvent molecules and the repulsive force between the charged particles prevent their aggregation.[1,31,92] Such a complexation process will override the effects of refractive index since it alters the electron density of the nanoparticle surface, thereby directly affecting the surface plasmon absorption band.

The surface plasmon absorption band of metal nanoclusters is very sensitive to the surface-adsorbed species and dielectric of the medium. For example, chemisorbed I^-, SH^-, and $C_6H_5S^-$ ions results in dampening of the surface plasmon band of colloidal silver particles.[93,94] Alternatively one can also observe bleaching of the surface plasmon band with electrons deposited from radiolytically produced radicals which cause a blue-shift and narrowing of the plasmon band.[95] A more detailed discussion on the damping effects caused by surrounding material can be found elsewhere.[77,82,96]

IV. Direct Excitation of the Metal Nanoparticles

A number of interesting phenomena have been observed with metal colloids under UV and visible light irradiation. The electronic excitation associated with direct excitation of the metal nanoclusters has been probed by pump−probe spectroscopy. In contrast to the bulk metal property, colloidal metals (e.g., gold) have been shown to be photoluminescent.[97−99] For example, gold nanorods exhibit an enhancement of 10^6 in the photoluminescence yield as compared to the bulk metal.[98] Many interesting nonlinear optical phenomenon[100,101] as well as surface-enhanced Raman scattering effects[65,66,70,74,75,102−104] are observed with silver and gold nanoparticles. Examples discussed in the following sections highlight laser-induced processes in gold and silver nanoparticles.

a. Transient Bleaching of the Surface Plasmon Band. The visible absorption bands of the gold (∼530 nm) and silver (∼380 nm) colloids make them ideal candidates to probe the optical effects by transient absorption[105−107] and transient grating spectroscopy.[108] Optical limiting and nonlinear optical properties of metal colloids have also been explored recently.[100,101,108,109] When the metal colloids are excited with a short laser pulse, a prompt bleaching of the plasmon band is observed within the laser pulse duration. The difference absorption spectrum of gold colloids shown in Figure 3 exhibits an intense bleaching of the surface plasmon band at 520 nm. The plasmon band of metal nanoparticles as explained on the basis of Mie theory involves dipolar oscillations of the free electrons in the conduction band that occupy energy states immediately above the Fermi level.[77,110] Once these electrons are excited by a laser pulse, they do not oscillate at the same frequency as that of the unexcited electrons, thus resulting in the decrease of the plasmon absorption band. These aspects have been addressed in recent spectroscopic investigations.[105,108,111,112] The recovery of the plasmon band at the picosecond time scale arises from the electron−phonon and phonon−phonon relaxation. Similar transient bleaching is seen for silver nanoparticles[106,113] and bimetallic particles.[114−116]

The bleaching recovery of the pristine Au colloids consists of a fast ($\tau = 2.5$ ps) and a slow process ($\tau > 50$ ps).[111] The

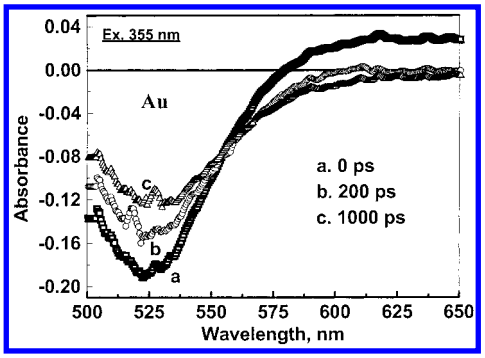

Figure 3. Time-resolved difference absorption spectra recorded following 355 nm laser pulse (pulse width 20 ps) excitation of 0.12 mM Au colloidal suspension.

SCHEME 4: Photoinduced Fusion and Fragmentation of Metal Nanoparticles

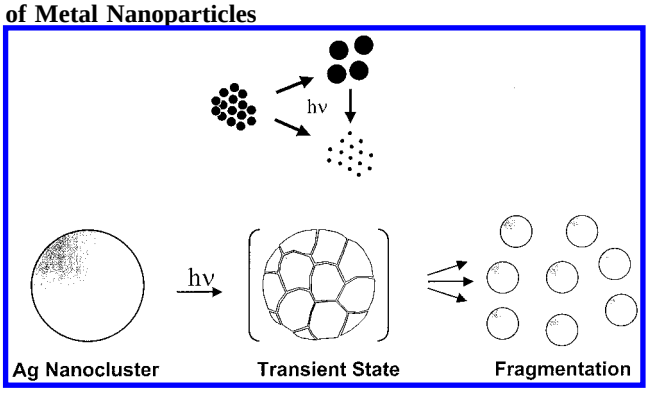

slower component of the recovery had a lifetime of 170 ps. These fast and slow recoveries correspond to the relaxation of "hot" electrons via electron−phonon coupling and phonon−phonon relaxation of the lattice, respectively. Dumping thermal energy into the solvent causes the dielectric of the surrounding medium to change, which in turn, influences the plasmon resonance frequency of the metal nanoclusters.

b. Laser-Induced Morphological Changes. Silver and gold nanoparticles show significant photoactivity and undergo morphological changes under laser irradiation.[39,48,51,113,117−121] These two possibilities are illustrated in Scheme 4. While these fragmentation and photofusion processes are found to be biphotonic and require high-intensity laser excitation, simple shape changes can occur at low intensity excitation. Two examples related to these photoinduced phenomena are presented below.

Photofragmentation of Silver Nanoclusters. The absorption spectrum of the silver colloids of facetted silver nanocrystals (particle diameter 40−60 nm) shows a surface plasmon absorption band with a maximum around 420 nm. This absorption band is rather broad and red-shifted compared to the plasmon absorption band of spherically shaped silver colloids prepared by radiolysis and other reduction methods. The 355 nm laser pulse excitation of the facetted silver nanocrystals induces a blue shift in the absorption spectrum. The absorption change was accompanied by a narrowing of the surface plasmon band and an increase in the magnitude of absorption. The blue shift and increase in the oscillator strength of the surface plasmon band is indicative of a decrease in particle diameter. Transmission electron micrographs recorded before and after the laser pulse excitation (Figure 4) shows that the relatively large (40−60 nm) silver particles fragment to produce smaller size (∼5 nm diameter) particles.

The photofragmentation of silver colloids was probed by time-resolved transient absorption experiments in a picosecond laser

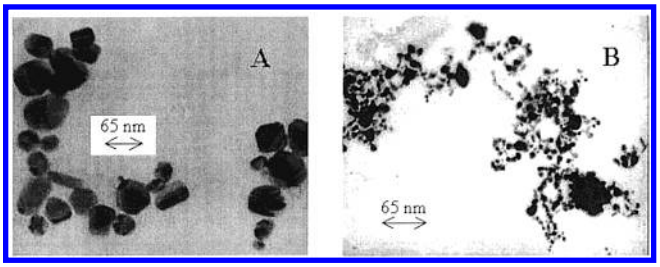

Figure 4. Transmission electron micrographs (TEM) recorded with a magnification 150000X: (A) Ag colloids prepared with citric reduction method and (B) same colloidal suspension after photolysis with 355 nm (1.5 mJ, 10 Hz) laser excitation for 3 min. (Reprinted with permission from ref 113. Copyright 1998 American Chemical Society.)

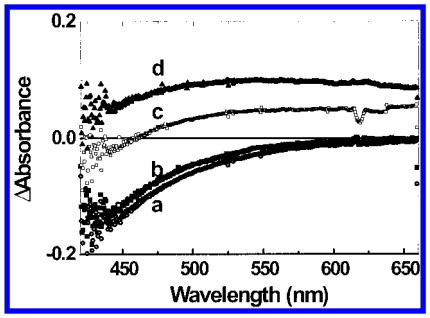

Figure 5. Time-resolved difference absorption spectra of 5.1×10^{-4} M colloidal Ag suspension in water (deaerated) (355 nm laser pulse excitation, 1.4 mJ, pulse width 20 ps). The transient spectra were recorded at delay times (a) 250 ps, (b) 500 ps, (c) 1250 ps, and (d) 2500 ps. (Reprinted with permission from ref 113. Copyright 2002 American Chemical Society.)

flash photolysis apparatus (Figure 5). Transient absorption spectra recorded at early times show transient bleaching at the surface plasmon band (400 nm). However, at longer delay times we see an increased absorbance in the red region. These transient absorbance changes are indicative of the optical effects arising from fragmentation of larger silver nanocrystals. The transient intermediate of the fragmentation process, which is monitored at 600 nm, shows a growth time of 1.5 ns (Figure 6). This transient is essentially an aggregate of smaller clusters that are in close proximity. The time constant of 1.5 ns corresponding to the absorption growth in Figure 6 shows the time frame with which chemical and physical changes occur in the parent Ag cluster following the laser pulse excitation. This transient aggregate then dissociates to generate stabilized smaller Ag nanoclusters. The 14.2 ns decay component of the transient absorption at 600 nm (Figure 6) corresponds to the time frame with which the fragmented clusters stabilize in solution. These smaller clusters possess properties that are exclusive to smaller size particles (e.g., exhibiting a 400 nm plasmon band maximum).

Photofusion of Metal Nanoclusters. A different scenario becomes evident if metal nanoparticles exist in the form of aggregates. Surface neutralization of citrate-stabilized gold nanoparticles with thiols readily yields clustered aggregates with broad absorption in the infrared. For example, the purple-colored gold colloidal solution turns blue as we add small amounts of thionicotinamide (TNA). Upon laser pulse (532 nm) irradiation of TNA-capped gold nanoparticle suspension for few minutes, the ruby-red color is restored as the aggregates fuse to form larger segregated spherical particles. In an independent study, El Sayed and co-workers[118,122,123] have observed laser-induced melting of gold nanorods into spherical particles.

The morphological changes caused by the laser irradiation of TNA-capped gold nanoparticle samples are shown in

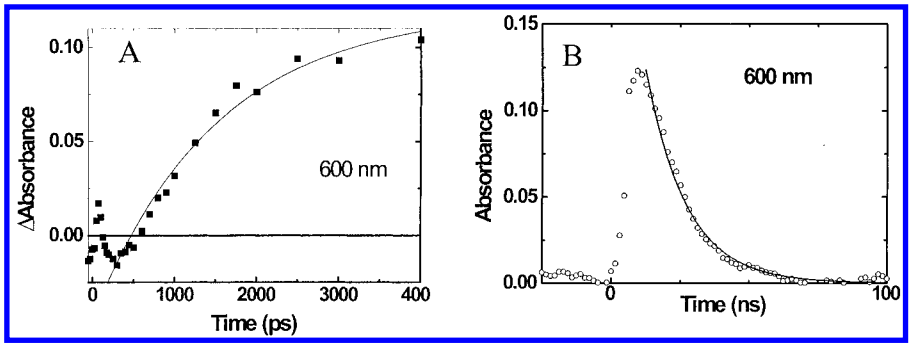

Figure 6. Growth and recovery kinetics of the transients generated following the 355 nm laser pulse (pulse width 20 ps) excitation of 5.1×10^{-4} M colloidal Ag suspension in water (deaerated). The monitoring wavelengths were (A) 440 nm and (B) 650 nm. (Reprinted with permission from ref 113. Copyright 2002 American Chemical Society.).

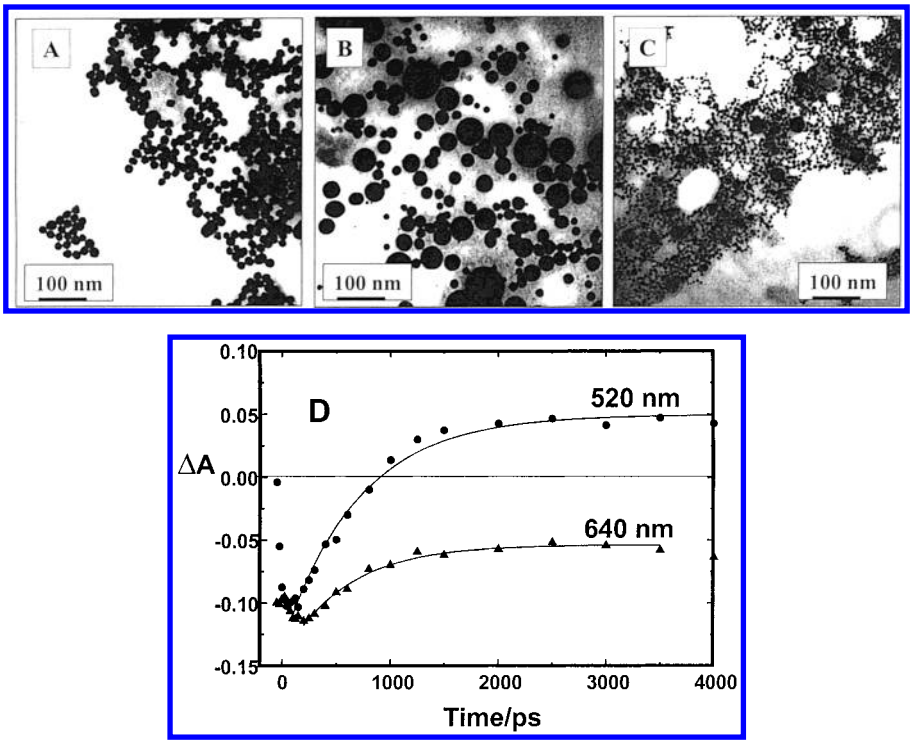

Figure 7. Transmission Electron Micrographs of TNA-capped gold colloids, (A) before, (B) 1 min, and (C) 30 min after 532 nm laser irradiation. (D) The absorption−time profiles recorded at (a) 520 nm and (b) 640 nm following the laser pulse (532 nm) irradiation of TNA-capped gold nanoclusters. (Reprinted with permission from ref 51. Copyright 1999 American Chemical Society.).

transmission electron microscopy (Figure 7). Native gold colloids prepared by citric acid reduction method are nearly spherical in shape with a particle diameter of 15−20 nm. The transmission electron micrograph of TNA-capped gold nanoparticles (Figure 7A) shows the presence of cluster islands, each consisting of several nanoparticles that are in close contact. After one minute laser pulse irradiation (532 nm,10 Hz, 1.5 mJ) the aggregate sample transforms to form large size spherical particles.(Figure 7B). Pumping the laser pulses (532 nm) for a longer duration (15−30 min) results in the fragmentation of these fused particles (Figure 7C).

Since the bleaching of the aggregation band corresponds to the photofusion process, one can evaluate the evolution of the photofusion process using transient absorption spectroscopy (Figure 7D). The bleaching occurs within the laser pulse duration of 18 ps and recovers partially during the period of 1 ns. The residual bleaching represents the disappearance of aggregate band. On the same time scale a growth in the plasmon absorption (520 nm) is seen as a result of formation of segregated particles. Although these nanoclusters have grown in size (∼100 nm) during the fusion process, they are well-separated from each other, thus ceasing the aggregation effects on the absorption spectrum. No such changes were seen when unmodified gold colloids were subjected to laser pulse irradiation under similar experimental conditions.

Similarly, cationic dyes such as Rhodamine 6G induce aggregation as they bind to small gold nanoparticles (particle diameter 2−3 nm) in thiocyante medium.[124] The photochemical/photothermal activity of Au/Rh-6G cluster assembly was observed under visible laser excitation. Upon 532 nm laser pulse excitation, the gold−dye cluster aggregates undergoes fusion to yield larger gold particles (5−20 nm in diameter). As gold cluster aggregates grow in size during the laser irradiation, the surface area available for the binding of the dye decreases. This process, which occurs with a rate constant of 7×10^8 s^{-1}, causes ejection of a few dye molecules into the bulk solution.

The photofusion phenomenon occurs as a result of melting of aggregates to form larger spherical particles during laser irradiation. As the gold particles are repeatedly bombarded with laser pulse, the temperature of these particles increases and causes melting of these particles. Theoretical calculations have predicted a rise in temperature up to 2500 K during laser

excitation.[125] Similar laser-induced fusion is not seen in uncapped gold colloids because individual particles are well-separated and the heat gained from laser excitation is quickly dumped into the surrounding aqueous medium (<200 ps).[112,126,127]

Gold-capped TiO_2 nanocomposite clusters were also found to undergo photoinduced fusion following 532 nm laser pulse excitation.[120] To observe fusion it is necessary to keep these clusters in the aggregated form. For high $[TiO_2]$:[Au] ratio, the clusters are well-dispersed with no noticeable changes in the shape of these composite clusters. The clustering of aggregates observed at low TiO_2:Au ratio ($[TiO_2]$:[Au] $\leq$ 1:1) facilitates dramatic morphological changes as they melt and fuse to form larger composite nanoclusters. Laser-induced melting/fusion was confirmed from the growth in the particle size as well as the disappearance of the aggregation absorption band. The process of melting and fusion occurred with an apparent rate constant of 1.25×10^9 s^{-1}. Whereas the laser-induced fusion is a unique way to synthesize multicore/shell composite nanoparticles, direct applications of these systems remain to be explored. Further details on the melting of metal nanoparticles and nanorods can be found in the published work of El-Sayed and co-workers.[119,122,123,128,129]

V. Chemical Binding of Gold Nanoparticles with Photoactive Molecules

Ways to organize metal nanoparticles into controlled architectures are becoming increasingly important in developing next generation nanodevices.[17,31,130−133] Of particular interest is the possibility of tailoring the metal nanocluster surface with a three-dimensional molecular arrangement consisting of electro- and photoactive moieties (Scheme 2). Researchers have often used functional groups such as thiols, amines, or silanes to attach electroactive or photoactive molecules to the gold surface.[134−138] The ability of gold surfaces to bind with specific functional groups makes them potentially useful in the development of biological probes,[83,139−141] photonic materials,[142] and chemical sensors.[143,144] In a recent study, Fox and co-workers[145] have demonstrated the ability of gold nanoparticles to preserve the photoreactivity of the *trans*-stilbene and *o*-nitrobenzyl ether moieties similar to the one observed in solution phase. Such photoactive metal nanoparticles are important for designing light-energy-harvesting devices of nanometric dimension and photocatalysts.

An inorganic−organic hybrid probe also offers the possibility of using complementary sensing via fluorescence spectroscopy and electron microscopy. Since fluorescence spectroscopy is a very sensitive technique, fluorophore bound gold nanoparticles are useful probes for biomolecular labeling (e.g., as immunoprobes).[16,139,140] Assembling fluorophore-metal nanoparticle superstructures as a two- or three-dimensional architecture provides routes to design novel materials with tailored electrical,[146] optical,[147−149] lithographic,[70,150−154] sensing,[143,155−159] and photochemical[145,160−164] properties. To meet the practical challenges that lie ahead, we need to understand surface interactions at the molecular level and develop strategies of refining properties of nanoparticle superstructures.

Efforts to extend the chemical functionalization concept to gold nanoparticles in aqueous and nonaqueous media is often encountered with the stability problems. Surface charge neutralization, which accompanies the binding of a thio or amine group to gold nanoparticles, induces aggregation and shifts the absorption to the infrared.[51] However, careful control of synthetic approach can facilitate organizing fluorophore molecules on the gold nanoparticles without inducing such aggregation effects.

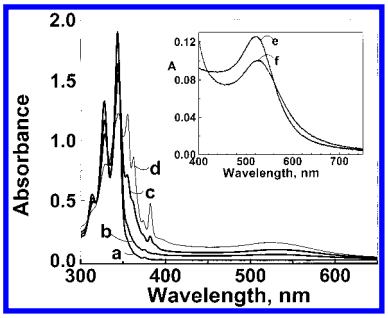

Figure 8. Effect of gold concentration, (Au) on the changes in the absorption spectrum of Py-CH_2NH_2 [60 μM] in THF: (a) 0, (b) 20.3, (c) 27, and (d) 47 μM of Au. Inset shows the absorption spectra of 34 μM of Au in the absence and presence of 20 μM Py−CH_2NH_2. All solutions contain 2.4 mM of tetraoctylammonium bromide (TOAB). (Reprinted with permission from ref 175. Copyright 2000 American Chemical Society.)

a. Surface Complexation with Organic Molecules. Interaction with such chemical species alters the electron density of the gold nanoparticles on the metal surface, thereby directly affecting the absorption of the surface-bound organic moiety as well as surface plasmon absorption band.[82,93,165] Figure 8 shows the spectral changes associated with the complexation of pyrene methylamine with gold nanoparticles. THF solution of Py−CH_2NH_2 possesses well-defined absorption bands in the UV region (313, 327.5, and 343.5 nm) corresponding to the monomer form of the pyrene chromophore (trace a, Figure 8). Upon addition of gold colloids, new absorption bands appear at 354, 361, 373, and 382 nm with a concomitant decrease in the monomer absorption bands of Py−CH_2NH_2. The changes in the absorption spectrum reflect the alteration of the electronic properties of the pyrene chromophore as it binds to the gold nanoparticle. The observation of isosbestic points at 319, 331, 338, and 347 nm in the absorption spectra recorded at varying gold nanoparticle concentrations confirms the existence of two forms of Py−CH_2NH_2, viz., free and bound forms of Py−CH_2-NH_2.

Surface functionalization of metal particles also leads to the dampening and broadening of its surface plasmon band. One can utilize these spectral shifts to measure the binding constants of fluorophores with gold and silver nanoparticles. Dampening and broadening of the surface plasmon band was evident as these molecules complexed with the gold surface. For example, complexation between gold nanoparticle and phenyl isothiocyanate (PITC) results in the blue-shift of absorption maximum of ~10 nm. The intensity of plasmon band decreases at 521 nm as we increase the concentration of PITC. The difference spectra shown in Figure 9 highlight the spectral differences arising as a result of varying the concentration between complexed and uncomplexed gold nanoparticles. Presence of an isosbestic point at 570 nm also confirms that these absorption changes arise from a complexation equilibrium (eq 3).

$$(Au^0)_n + \mathrm{PITC} \leftrightarrow [(Au^0)_n \cdots \mathrm{PITC}] \qquad (3)$$

The association constant for the complexation between Au nanoparticle and PITC were obtained by analyzing the absorption changes in Figure 9 similar to a Benesi−Hildebrand approach.[166] An apparent association constant of 5×10^4 M^{-1} was obtained from the double reciprocal plot of $1/\Delta A$ versus 1/[PITC] (inset in Figure 9). The high value of K_{app} observed in these experiments suggests a strong association between the gold colloids and PITC. Similar spectral changes were also observed when gold nanoparticles were complexed with ^{15}N-

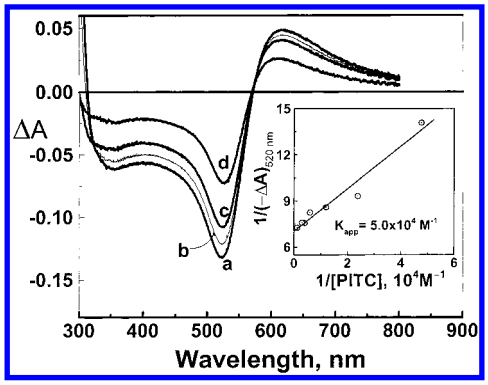

Figure 9. The difference absorption spectra highlighting the spectral changes associated with complexation in TOAB/toluene solution. The concentration of PITC was varied from 20 to 150 μM. Inset shows the dependence of $1/\Delta A$ versus 1/[PITC] (Reprinted with permission from ref 40. Copyright 2002 American Chemical Society.)

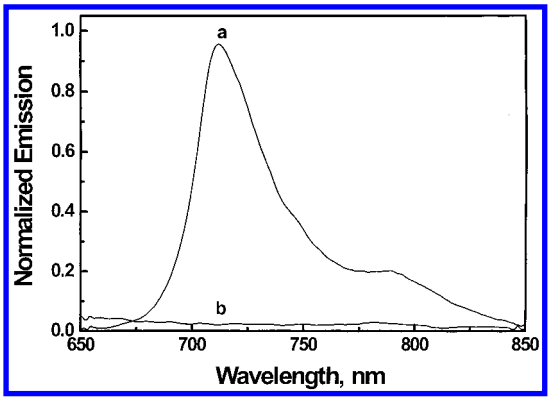

Figure 10. Fluorescence emission spectra of the optically matched solutions of the (a) fullerene thiol and (b) (Au−S−C_{60} in toluene. (excitation wavelength, 470 nm) (Reprinted with permission from ref 188. Copyright 2002 American Chemical Society.)

labeled benzylamine with similar high apparent association constant ($\sim 5 \times 10^4$ M^{-1}) as that of gold−PITC equilibrium.

b. Dye-Capped Metal Nanoclusters. Close packing of the dye molecules on a charged particle surface often leads to aggregation effects.[167−169] Such dye aggregates are capable of interacting with the support material when subjected to photoexcitation. To date, most of these studies are limited to semiconductor nanocluster systems. There is a great deal of interest in understanding the interactions between the organic dye and metal nanoclusters and the effect of excited-state quenching and surface-enhanced Raman emission of the surface bound dye molecules.[102,170] Often excited-state quenching of the dye molecules on metal surfaces is attributed to the energy-transfer process.[134,138,147,171,172]

For silver particles coated with Rhodamine 6G, a blue shift has been observed for both the silver surface plasmon band and the dye visible absorption band.[173] Metal nanoclusters (copper, silver, and gold) embedded in a copper phthalocyanine matrix have been shown to enhance nonlinear optical processes.[174] Makarova et al.[138] and Templeton et al.[31] have modified the surface of gold nanoparticles with fluorescein isothiocyanate. They showed the possibility of adsorbing dye molecules onto the gold particle surfaces without inducing any aggregation effects.[138] Fundamental understanding of such events becomes important if one hopes to use metal nanoclusters or composite assemblies for optoelectronic or light energy conversion devices. A cationic dye such as rhodamine 6G undergoes H-type aggregation when bound to small gold nanoparticles. The photochemical/photothermal activity of Au/Rh-6G cluster assembly has been successfully demonstrated using visible laser excitation.[124]

c. Photoinduced Energy and Electron-Transfer Process between Excited Sensitizer and Metal Nanocore. Binding of a photoactive or fluorophore molecule such as pyrene to a gold nanoparticle renders the organic−inorganic hybrid nanoassemblies suitable for light-harvesting and optoelectronic applications.[133,175] Photoinduced electron transfer and energy transfer in a number of donor−acceptor systems have been extensively studied with an aim to mimic natural photosynthesis, by converting the charge-separated state into chemical or electrical energy.[176,177] By suitably assembling these systems on a metal surface one can find ways to utilize the separated charge in such molecular assemblies. Demonstration of such a concept is made using self-assembled monolayers (SAMs) of photoactive molecules on gold electrodes.[60,145,155,161,172,178−185] Direct binding of a fluorophore to the metal surface often results in the quenching of excited states.[138,171,172,186] Both energy-transfer and electron-transfer processes are considered to be major deactivation pathways for excited fluorophores on metal surfaces. Examples of gold nanoparticles functionalized with thiol-derivatized fullerene and pyrene (Scheme 5) are presented here to discuss the excited-state deactivation pathways in metal-sensitizer systems.

Au−SR−C_{60} System. Fullerene-functionalized gold clusters can be visualized as self-assembled photoactive antenna systems containing gold nanoparticle as central nanocore and appended fullerene moieties as the photoreceptive hydrophobic shell (Scheme 5). Such molecular−gold nanoassemblies can serve as important building blocks in the design of light-harvesting systems.[187,188] In the absence of gold nanoparticles, the emission spectrum of fullerene thiol in toluene shows a maximum at 710 nm, which corresponds to its singlet excited state. These spectral profiles of fullerene thiol emission (trace *a* Figure 10) were found to be similar to those of the previously reported clusters of functionalized C_{60} molecules.[189,190] The major deactivation pathway for the excited singlet is the intersystem crossing to generate triplet excited state.

Interestingly, the fullerene thiol emission is totally quenched when it is anchored on the gold nanocore. This observation shows that the decay of singlet excited fullerene moieties is affected by its binding to gold nanocore. The quenching of singlet emission would result from either the enhanced intersystem-crossing efficiency or by direct energy transfer from excited fullerene moiety to the gold nanocore (reactions 4−6).

$$\text{Au}-\text{S}-\text{C}_{60} + h\nu \rightarrow (\text{Au}-\text{S}-{}^1\text{C}_{60}^*) \quad (4)$$

$$(\text{Au}-\text{S}-{}^1\text{C}_{60}^*) \rightarrow (\text{Au}-\text{S}-{}^3\text{C}_{60}^*) \quad (5)$$

$$(\text{Au}-\text{S}-{}^1\text{C}_{60}^*) \rightarrow (\text{Au}^*-\text{S}-\text{C}_{60}) \quad (6)$$

Moreover, an additional deactivation pathway that involves electron transfer between excited fullerene and gold nanocore could also contribute to the fluorescence quenching of fullerene thiol.

To establish the excited-state-deactivation pathways, we recorded transient absorption spectra (Figure 11) following the 337 nm laser pulse as the excitation of fullerene thiol solution. The excited fullerene thiol in toluene shows an absorption band at 700 nm, which is characteristic of triplet excited fullerene moiety. A majority of excited fullerene triplets studied so far, show relatively less pronounced band in the near UV region. However, for fullerene thiol triplet, we observe another prominent UV band at 360 nm with an extinction coefficient similar

SCHEME 5: Au−S−C_{60} (left) and Au−S−Pyrene (right) Nanoassemblies

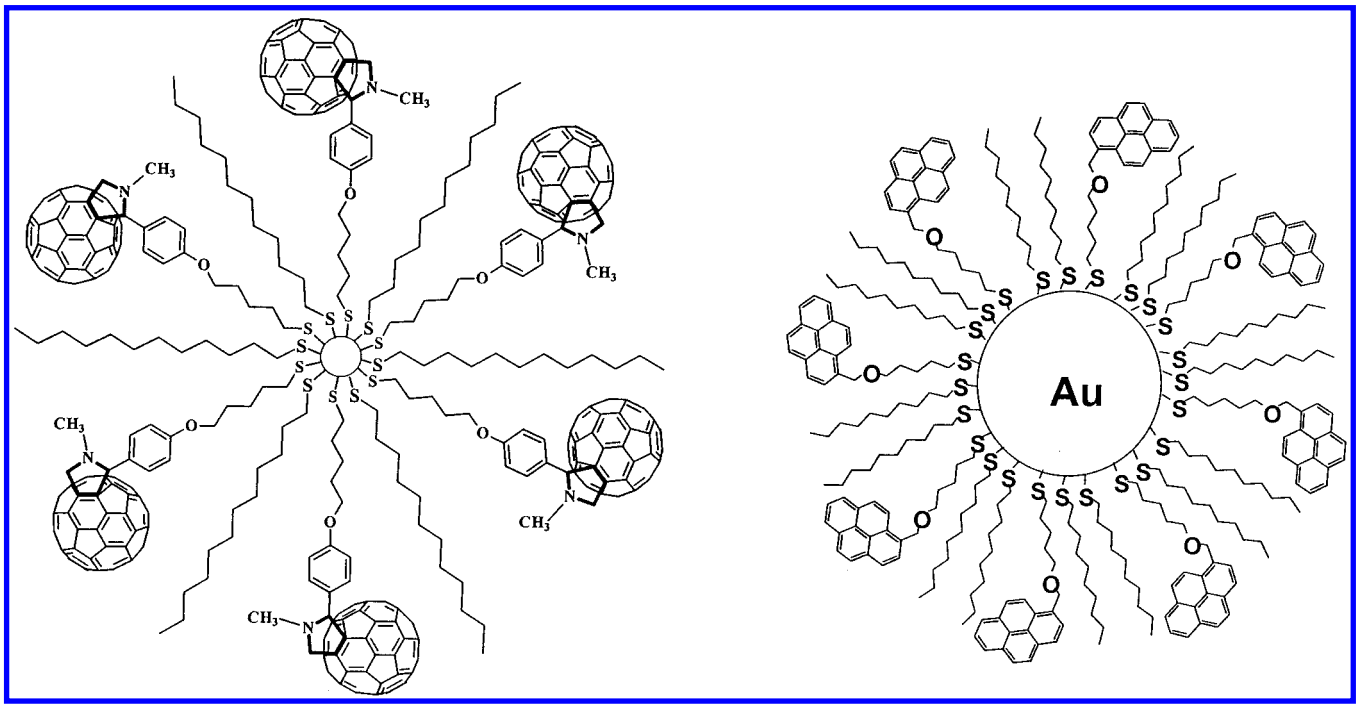

to that of 710 nm band. The transient absorption decay at 710 and 380 nm follow the first-order kinetics with a lifetime of 16.7 and 14.3 μs, respectively (Figure 11 inset). The similarity of transient decay lifetimes at these two absorption bands confirms that triplet excited species is the only long-lived transient formed following the excitation of fullerene thiol.

The transient absorption spectrum recorded following the excitation of Au−S−C_{60} exhibit relatively weak absorption throughout the UV−vis region. The transient studies did not indicate the formation of any electron-transfer products for the Au−S−C_{60} system. These results indicate that the electron-transfer process is not a major deactivation pathway for the excited fullerene on gold surface. Low yields of singlet and triplet of fullerene moiety in excited Au−S−C_{60} assembly confirm that most the excited energy of the fullerene moiety is quickly dissipated, following the excitation via energy transfer to the gold nanocore.

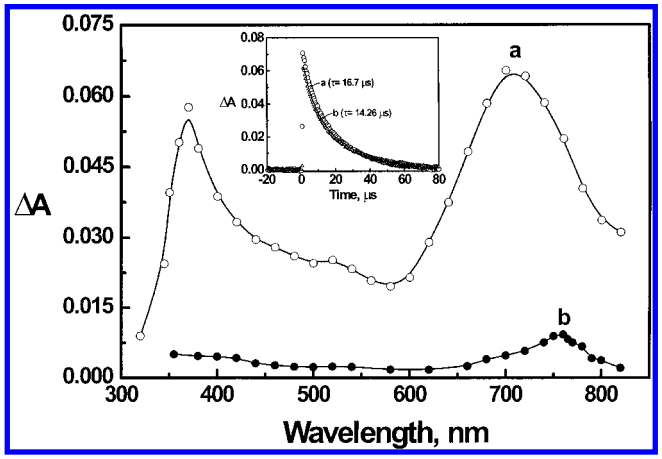

Figure 11. Transient absorption spectra recorded 2.5 μs after 337 nm laser pulse excitation of degassed toluene solutions of (a) fullerene thiol and (b) Au−S−C_{60}. Inset shows the decay of the triplet excited fullerene thiol monitored at (a) 710 and (b) 380 nm, respectively. (Reprinted with permission from ref 188. Copyright 2002 American Chemical Society.)

Au−S−Pyrene System. Indirect evidence for electron transfer between the chromophore and the gold surface has been obtained from photocurrent measurements.[164,184] Obtaining insight into such processes using spectroscopic measurements becomes important if one is interested in improving the charge separation efficiencies in gold-fluorophore nanoassemblies. Recent transient absorption studies relate the excited-state quenching of the surface-bound fluorophores to an electron-transfer process in the pyrene thiol-bound gold (Au−SR−Py) nanoassemblies.[191]

Au−SR−Py assemblies exhibit absorption and emission properties that are characteristic to the pyrene moiety (Figure 12 A,B). The absorption in the 300−350 nm region show three distinct absorption bands (313, 328, and 345 nm) corresponding to the absorption of pyrene. The emission spectrum shows maxima at 376, 382, and 395 nm and a broad band in the 475 nm region. The intensity of these three peaks in the absorption and emission spectra often serves to sense the polarity of the microenvironment.[192] The prominence of peak III over peak I (395 nm emission band over 376 nm band in Figure 12B) suggests the immediate surroundings of the gold−fluorophore nanoassembly to be highly nonpolar. The decreased fluorescence yield confirms that a large fraction of excited pyrene molecules are quenched by the gold nanocore.

Figure 13 shows the transient absorption spectra of HS−Py and Au−SR−Py in degassed and air-saturated THF solutions. The difference absorption spectrum recorded following 337 nm laser pulse excitation of HS−Py in degassed THF solutions exhibits a maximum around 425 nm. This absorption band is characteristic of triplet−triplet absorption of pyrene and is readily quenched in oxygenated solutions. On the other hand the transient absorption spectrum recorded following 337 nm laser pulse excitation of Au−SR−Py shows the formation of a transient with absorption maximum at 400 nm which we attribute to the pyrene cation radical. Time-resolved spectra recorded at different times confirm the presence of a single transient, which decays with a lifetime of 4.5 μs. The presence of O_2 in the solution has no effect on the formation or decay of the 390 nm transient formed following the excitation of

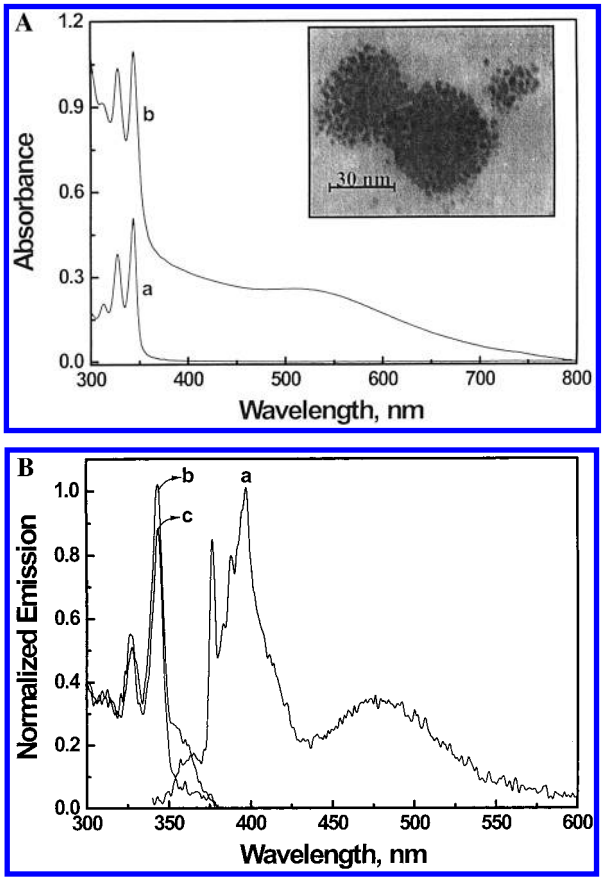

Figure 12. (A) Absorption spectra of (a) pyrene thiol and (b) Au−SR−Pyrene in THF. The inset shows the Transmission Electron Micrograph of Au−SR−Pyrene deposited on a copper grid. (B) Emission spectrum of Au−SR−Pyrene in THF (λ_{exc}= 325 nm). (b and c) Excitation spectra of Au−SR−Pyrene in THF at monitoring wavelengths 390 and 500 nm, respectively. (Reprinted with permission from ref 191. Copyright 2002 American Chemical Society.)

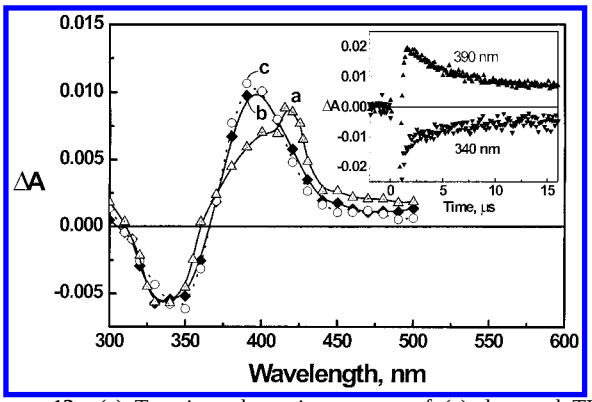

Figure 13. (a) Transient absorption spectra of (a) degassed THF solution of pyrene thiol, (b) degassed THF solution of Au−SR−Pyrene, and (c) oxygenated THF solution of Au−SR−Pyrene. All spectra were recorded 2 μs after 337 nm laser pulse excitation. Inset shows the absorption-decay profiles recorded at 400 and 340 nm. (Reprinted with permission from ref 191. Copyright 2002 American Chemical Society.)

Au−SR−Py (spectrum c in Figure 13). Thus, the properties of the transient observed with Au−SR−Py are distinctly different from those recorded with pyrene thiol solution. These transient properties confirm the formation of pyrene cation radical. Furthermore, the absence of triplet excited state in spectrum b (Figure 13) supports the hypothesis that the metal nanocore is responsible for suppressing the intersystem crossing and/or total quenching of the triplet excited state and facilitates photoinduced electron transfer in the Au−SR−Py system.

The decay of the transient absorption at 390 nm and recovery of bleaching at 340 nm (see absorption−time profiles in the inset of Figure 13) show a similar first-order kinetics with lifetimes of 4.7 and 4.4 μs, respectively. The similarities between these two processes suggest that the decay of the pyrene cation radical corresponds to the recovery of parent fluorophore via a back electron-transfer process (reaction 7).

$$\text{Au(e)}-\text{SR}-\text{Py}^{+\bullet} \rightarrow \text{Au}-\text{SR}-\text{Py} \qquad (7)$$

As shown earlier, thiol-capped gold nanoparticles are capable of holding the charge in a quantized fashion.[132,193−195] Photochemical electron storage in colloidal metal was demonstrated by hydrogen evolution reactions.[196] In the example discussed above, the ability of gold nanocore to accept charge from the excited pyrene makes the charge separation possible. It is interesting to note that this charge separation is sustained for several microseconds before undergoing recombination. The ability of gold nanoparticles to participate photoinduced electron-transfer reactions demonstrates the possibility of employing fluorophore-bound gold nanoparticles as light-harvesting assemblies. Fox and co-workers[197] have confirmed the photoinduced electron transfer from excited pyrene in a self-assembled monolayer of sulfur-terminated oligonucleotide duplexes on flat gold surfaces is from photocurrent generation. Similar photocurrent studies involving chromophores on gold surfaces have also been carried by other researchers.[164,185]

d. Enhancing the Emission of a Surface-Bound Fluorophore. As discussed in the previous section organic-capped gold nanoparticles are good electron acceptors and are capable of storing charge in a quantized fashion. If indeed the gold particle acts as an electron acceptor, it should be possible to modulate the electron-transfer quenching of the excited fluorophore by charging the gold nanoparticle by alternate means. One such possibility of charging of organic-capped gold nanoparticles is to employ an electron rich amine functional group as the linker between fluorophore (e.g., pyrene) moiety and the gold nanocore (Scheme 6).[175]

The TOAB-capped gold nanoparticles are nonfluorescent and Py−CH_2NH_2 in THF exhibits weak florescence (ϕ_f = 0.09) with emission maxima at 377 and 397 nm. On the other hand the Py−CH_2NH_2 molecules bound to gold nanoparticles exhibit strong emission bands at 383 and 403 nm (Figure 14). The red shift in the emission peaks parallels the shift in absorption bands (see Figure 8). These new electronic transitions of the pyrene chromophore become allowed as the amine group binds strongly to the gold particle. No such spectral shifts or enhanced emission could be seen when we added a THF solution containing tetraoctylammonium bromide and treated with $NaBH_4$ (i.e., excluding gold nanoparticles from the solution). Katz and co-workers[198] have observed a 26-fold enhancement in the fluorescence yield of pyrene molecules upon their binding to gold nanoparticles via a thioester or thiocarbonate linkage. Evidence for the chain density gradient and the motion of termini groups of alkanethiolates adsorbed onto the surface of gold nanoparticle has recently been obtained from the fluorescence enhancement during aging of the sol.[199]

The observed increase in the fluorescence yield therefore reflects the suppression of the nonradiative decay processes upon binding to gold nanoparticles. The low fluorescence yield of Py−CH_2NH_2 in THF is attributed to the intramolecular quenching of the singlet excited state.[175] The photoinduced electron transfer between the lone electron pair of amine and pyrene moieties competes with the radiative and nonradiative decay of the singlet excited state. Upon binding of the amino group

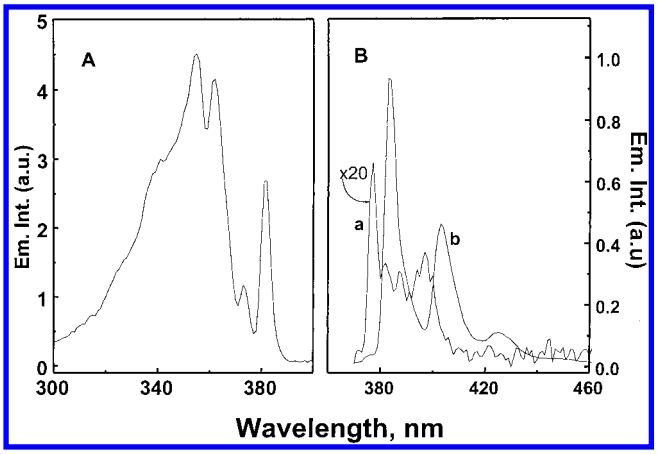

Figure 14. (A) The excitation spectrum of Py−CH_2NH_2 bound gold nanoparticles (emission was followed at 410 nm). (B) The emission spectra of (a) Py−CH_2NH_2, (b)Py−CH_2NH_2 bound gold nanoparticles in THF (excitation wavelength were 321 and 361 nm, respectively. The intensity of the emission spectra of unbound Py−CH_2NH_2 has been multiplied by a factor of 20 for the purpose of comparison.) All solutions contain 2.4 mM of tetraoctylammonium bromide (TOAB). (Reprinted with permission from ref 175. Copyright 2000 American Chemical Society.)

SCHEME 6: Charging of Gold Nanocore with the Donation of Lone-Pair Electron Results in the Stabilization of Excited State

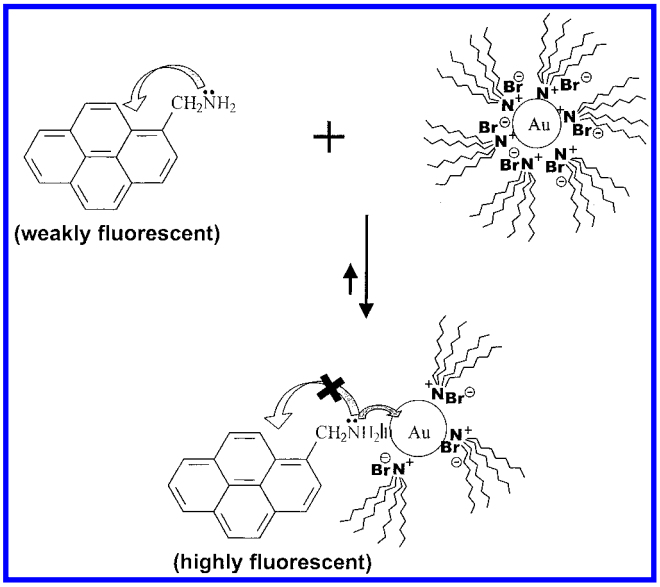

to the gold surface, the electron-donating ability of the amine group is decreased and this in turn suppresses the electron transfer from its lone pair to the pyrene moiety. A similar chelation-enhanced fluorescence has been reported earlier by Czarnick and co-workers[200,201] and de Silva and co-workers.[202,203] Binding metal cations to amine functional groups of probes (e.g., anthracene), they were able to demonstrate the suppression of intramolecular quenching. A fluorescence enhancement of a fluorophore (pyrene) on a gold nanoparticle surface has also been achieved recently in our laboratory by suppressing the charge-transfer quenching with externally applied electrochemical bias.[204]

VI. Semiconductor−Metal Nanocomposites in Photocatalysis

One of the major goals behind designing semiconductor−metal composite nanoparticles is to improve the catalytic

SCHEME 7: Improving the Interfacial Charge-Transfer Processes in Metal-Capped Semiconductor Particles

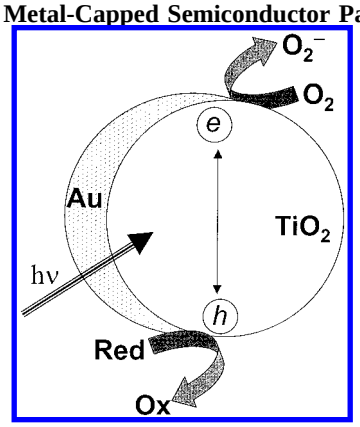

SCHEME 8: Synthesis of Metal-Capped Oxide Particles

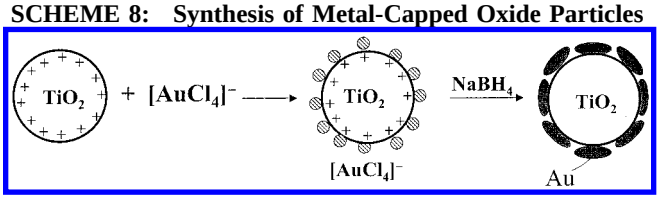

properties or to tune the luminescent or sensing properties (Scheme 7). Contact of metal with the semiconductor indirectly influences the energetics and interfacial charge transfer processes in a favorable way. For example single component semiconductor nanoparticles exhibit relatively poor photocatalytic efficiency (<5%) since the majority of the photogenerated charge carriers undergo recombination.[205] Semiconductor−metal composite nanoparticles on the other hand facilitate charge rectification (i.e., directing the flow of electrons and holes in opposite directions) and improve the photocatalytic efficiency in these systems. The deposition of a noble metal on semiconductor nanoparticles is an essential factor for maximizing the efficiency of photocatalytic reactions.[206,207] The noble metal (e.g., Pt), which acts as a sink for photoinduced charge carriers, promotes interfacial charge-transfer processes. A direct correlation between the work function of the metal and the photocatalytic activity for the generation of NH_3 from azide ions has been made for metallized TiO_2 systems.[208] Composite semiconductor systems have also been shown to improve the photoconversion efficiency of dye-sensitized photochemical solar cells[209,210] and photocatalytic reactions.[211,212]

Despite several efforts to synthesize semiconductor/metal composite systems,[213−217] little information is available on the photodynamics of these materials. Fundamental understanding of the photoinduced interactions between a semiconductor and metal as well as the interfacial charge-transfer process in nanocomposites is important to elucidate the role of noble metals in semiconductor assisted photocatalysis. Recently, Halas and co-workers[53,218−220] have investigated the effect of an oxide core on the optical properties of gold nanoshell and chemically bound gold nanoparticles.

A simple method of preparing semiconductor−metal nanocomposites (represented as core@shell) involves reduction of the desired metal on preformed semiconductor nanoparticles (Scheme 8). For example, TiO_2@Au or SnO_2@Ag nanoparticles can be prepared by adding the desired amount of $HAuCl_4^-$ solution to the colloidal TiO_2 or $AgNO_3$ solution to SnO_2 suspension in water while stirring vigorously. The TiO_2 colloids prepared in acidic medium were positively charged while SnO_2 colloids in alkaline medium carried a net negative surface charge. Thus, $AuCl_4^-$ and Ag^+ ions can be attached to TiO_2

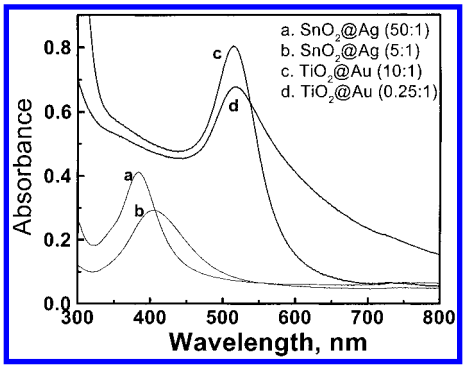

Figure 15. Absorption spectra TiO_2@Au and SnO_2@Ag colloids. The concentration of the metal shell was kept constant at 2×10^{-4} M Au and 5×10^{-5} M Ag in water containing different concentrations of TiO_2 and SnO_2, respectively (path length 1 cm). SnO_2:Ag ratio was maintained at (a) 50:1 and (b) 5:1 and TiO_2:Au molar ratio was maintained at (c) 10:1 and (d) 0.025:1. (Reprinted with permission from refs 116 and 120. Copyright 2001 American Chemical Society.)

and SnO_2 surfaces via electrostatic binding. Upon reduction with $NaBH_4$ we obtain a stable TiO_2@Au and SnO_2@Ag nanocomposite particles in water. The presence of metal oxide colloid is important for achieving the stability of the suspension. Gold (or silver) reduction carried out in the absence of TiO_2 (or SnO_2) core using same experimental procedure did not produce stable colloids. A similar approach has been adopted to synthesize metal-capped ZnO nanoparticles.[221]

In the solutions containing higher metal oxide core concentrations (i.e., at greater ratio of SnO_2:Ag or TiO_2:Au) a sharp and prominent absorption (spectra a and c in Figure 15) corresponding to the surface plasmon band of the corresponding metal is observed (viz., 520 nm for Au in TiO_2@Au and 390 nm for Ag in SnO_2@Ag colloids). However, for the colloids prepared using lower metal oxide concentrations (i.e., when the ratio of SnO_2:Ag or TiO_2:Au was kept low) we observe a dampening and broadening of the surface plasmon band and an appearance of aggregation band in the longer wavelength region (spectrum b and d in Figure 15). A red shift in the absorption maximum (405 nm) was also evident in the case of SnO_2@Ag colloids. The lack of available charged metal oxide core at low metal oxide:metal ratio disturbs the uniformity of metal distribution and induces aggregation effects.

TiO_2 nanoparticles undergo charge separation under band gap excitation (Eg = 3.2 eV) and participate in the redox processes at the interface. We employed a 337 nm pulsed laser as the excitation source for exciting TiO_2 colloids and initiating the redox reactions at the interface (reactions 8 and 9).

$$TiO_2 - h\nu \rightarrow TiO_2(e+h) \quad (8)$$

$$TiO_2(h) + SCN^- \rightarrow TiO_2 + SCN^{\bullet} - (SCN^-) \rightarrow (SCN)_2^{-\bullet} \quad (9)$$

The ability of photogenerated holes to oxidize thiocyanate ions at the semiconductor interface has been demonstrated earlier.[222] The transient spectrum recorded immediately after 337 nm laser pulse excitation of TiO_2@Au nanoparticles in aqueous SCN^- solution is shown in Figure 16. The spectral feature of this transient match the characteristics of the thiocyanate radicals ($(SCN)_2^{-\bullet}$) with an absorption maximum at 480 nm.[222,223] These thiocyanate radicals produced photocatalytically was found to complex with the gold surface (abs max 390 nm), the details of which can be found elsewhere.[224]

Since the formation of $(SCN)_2^{-\bullet}$ radicals immediately after the laser pulse excitation represents the quantitative estimate

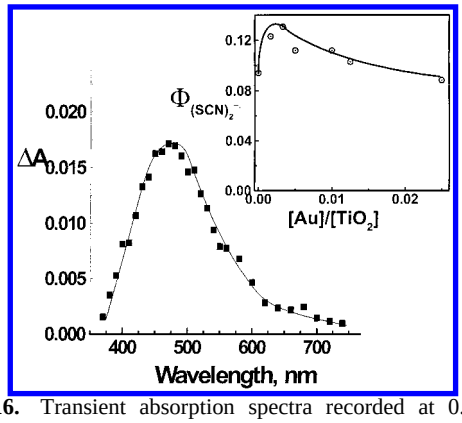

Figure 16. Transient absorption spectra recorded at 0.5μs after following 337 nm laser excitation of TiO2@Au (12 mM TiO_2 and 0.013 mM Au) colloidal suspension containing 25 mM NaSCN in aqueous solution. Inset shows the dependence of $(SCN)_2^{-\bullet}$ yield on the concentration of gold cap. The maximum absorbance at 480 nm was used to determine the quantum yield of oxidation process using benzophenone carboxylate as actinometry ref 237. (Reprinted with permission from ref 224. Copyright 2000 American Chemical Society.)

of the hole oxidation process, we monitored maximum absorbance at 480 nm at different TiO_2:Au ratios. (The TiO_2:Au ratio was varied by varying the gold concentration during sample preparation.) The inset of Figure 16 shows the dependence of $(SCN)_2^{-\bullet}$ yield on the gold shell concentration. In the absence of gold capping, TiO_2 colloids generate $(SCN_2)^{-\bullet}$ radicals with a quantum yield of 0.09. At low concentrations of gold we see an increase in the effeciency of oxidation process. For a [Au]:[TiO_2] ratio of 0.17 we see more than 40% enhancement in the oxidation efficiency ($\Phi(SCN)_2^{-\bullet} = 0.13$). As we further increase the Au concentration, the efficiency of thiocyanate oxidation at gold-capped TiO_2 nanoparticles decreases. Inability of the photogenerated holes to reach the electrolyte interface as well as increased absorption by the gold are the likely reasons for observing lower $(SCN)_2^{-\bullet}$ yield at higher capping concentrations of gold. On the other hand, when low concentrations of metal are used to cap the semiconductor core we can expect the outer layer to be discontinuous. Such a configuration of core shell particles (i.e., small metal islands deposited on the TiO_2 core) provides a favorable geometry for facilitating the interfacial charge transfer under UV irradiation. (It should be noted that a new band appears at 390 nm in the case of TiO_2@Au nanoparticles as the transient absorption corresponding to $(SCN)_2^{-\bullet}$ decayed. As confirmed in our pulse radiolysis experiments,[224] the 390 nm absorption band represents complexation between $(SCN)_2^{-\bullet}$ radicals and the gold surface which further results in the oxidation of gold layer). The thiocyanate oxidation discussed here represents an example that elucidates the photocatalytic oxidation in semiconductor/metal nanocomposites. Other examples (e.g., water oxidation, CO_2 reduction, and mineralization of azo dyes) illustrating the beneficial aspects of semiconductor/metal nanocomposite can be found in the literature.[38,225−231]

Photoelectrochemical studies[38,232] carried out by depositing gold nanoparticles on nanostructured TiO_2 films also exhibit enhanced photocurrent generation. Improved interfacial charge transfer at the semiconductor/electrolyte interface resulted in nearly 3 times enhancement of photocurrent generation and a shift in the apparent flat band potential. Although the TiO_2@Au interface may offer many complex scenarios, the photoelectrochemical and photocatalytic measurements support the argument that the metal nanoparticle deposition facilitates charge (electron) stabilization in nanostructured TiO_2 films and promote interfacial hole-transfer process. A similar decrease in the overvoltage of

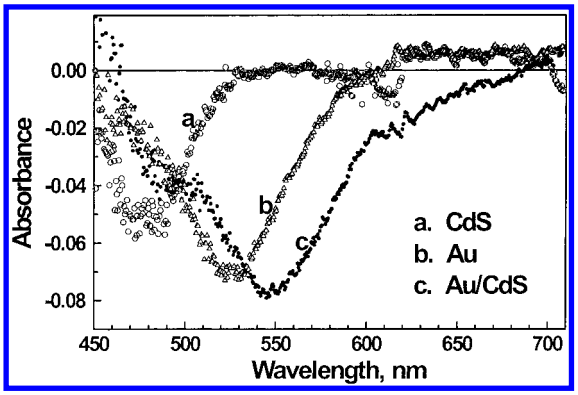

Figure 17. Transient absorption spectra recorded immediately after 355 nm laser pulse (pulse width 20 ps) excitation of colloidal suspension (degassed with N_2): (a) 0.25 mM colloidal CdS, (b) 0.12 mM Au, and (c) colloidal Au@CdS composite containing the same amount of Au and CdS as in (a) and (b) (Reprinted with permission from ref 127. Copyright 1997 American Chemical Society.)

the interfacial charge-transfer process has been noted earlier in semiconductor particle-assisted photocatalytic reactions[208] and p-GaAs[233] and p-Si[234] single-crystal-based photoelectrochemical cells. Adsorption of gold nanoparticles on TiO_2 films as scattered islands was also found to be sufficient to induce an enhancement in the photoelectrochemical performance.[232] Local photocurrent/voltage measurements have confirmed size-dependent barrier heights for the nanometal−semiconductor contacts.[235]

In another study, we probed the electron transfer between photoexcited CdS layer and gold core in a Au@CdS composite system using picosecond laser flash photolysis.[127] The transient absorption spectrum recorded following 355 nm laser pulse excitation of Au@CdS colloids shows two distinct transient bleaching maxima at 480 and 545 nm which correspond to the CdS shell and Au core, respectively. The difference absorption spectrum (spectrum c in Figure 17) observed in this set of experiments is different from the simple addition of the individual spectra a and b (Figure 17) recorded separately by exciting CdS and Au colloids. Since the absorbance of CdS at 355 nm is nearly twice that of Au colloids we expect CdS to absorb most of the excitation laser pulse in the composite system. Yet, the net bleaching of the CdS at 480 nm in the Au@CdS system is smaller than the CdS nanoclusters alone. On the other hand the surface plasmon absorption of the composite system is slightly more than that observed for the gold nanoclusters suspension. The photogenerated electrons in CdS nanoclusters are transferred to the Au core causing the surface plasmon absorption to bleach. This inter-particle electron transfer is completed within the laser pulse duration of 18 ps. While the surface plasmon bleaching in pristine gold colloids is seen with direct laser pulse excitation, the indirect process of electron injection mainly causes the bleaching at 545 nm in the Au@CdS composite. The former is due to heating of the electronic gas and the latter is due to the shift in Fermi level of gold core. The situation of electron injection in the Au@CdS core is similar to the one observed during the reaction of noble metal colloids with radiolytically generated radicals.[1,196] The slower recovery of the transient bleaching observed in the case of Au@CdS suggested improved charge separation in the Au@CdS composite system.

VII. Scope of Future Research

The photochemical and photocatalytic properties of various nanoassemblies discussed in this review article highlight the ways the metal nanoparticles interact with light. The ability to functionalize gold nanoparticles with photoactive molecules has opened new avenues to utilize these nanoassemblies in light energy conversion systems. By suitably modulating the fluorescence of the surface bound fluorophore these nanoassemblies can be tuned to design sensors, display devices and biological probes. Molecular architecture of inorganic and organic hybrid structure in future will play a crucial role in tailoring the requirements of new generation nanodevices.

Elucidation of the excited-state interactions with metal nanoparticles will continue to be a major research topic in the coming years. Understanding the properties of a surface bound molecule provides valuable information concerning the charge-transfer interactions as well as microsurrounding near the metal nanocore. Techniques such as single-molecule spectroscopy are expected to play an important role in elucidating the molecular level interactions. Exploring ways to improve photoinduced charge separation in donor−acceptor type dyads and triads by binding them to metal nanostructures and/or semiconductor composites will aid in mimicking artificial photosynthesis with improved efficiency.

The ability of gold nanoparticles in storing and shuttling of electrons has been demonstrated by monitoring molecule like charging effects[15,194] and Fermi-level equilibration with semiconductor nanostructures.[38,221,232] A thermally activated electron hopping from one gold particle to another has been proposed as a possible way of conducting charge through nanostructured gold films.[236] The mechanism of charge transport in metal nanostructures still remains an intriguing issue and needs to be explored further.

Organized nanoassemblies of organic molecules and inorganic nanoparticles after all are the building blocks of nanodevices, whether they are designed to perform molecular level computing, sense the environment or improve the catalytic properties of a material. The key to creation of these superstructures is to understand the chemistry at a fundamental level.

Acknowledgment. I thank Prof. Dan Meisel for many helpful discussions and Dr. K. George Thomas for initiating the work on fluorophore bound metal nanoparticles in organic media. I also acknowledge the contributions of research colleagues and students, N. Chandrasekharan, S. Barazzouk, V. Subramanian, H. Fujiwara, M. Flumiani, B. Shanghavi, and A. Dawson whose contributions are included in this review article. The research described here is supported by the Office of Basic Energy Science of the Department of the Energy. This is contribution no. NDRL 4374 from the Notre Dame Radiation Laboratory.

References and Notes

(1) Henglein, A. *J. Phys. Chem.* **1993**, *97*, 5457.
(2) Mulvaney, P.; Giersig, M.; Henglein, A. *J. Phys. Chem.* **1993**, *97*, 7061.
(3) Henglein, A. *Ber. Bunsen-Ges. Phys. Chem.* **1995**, *99*, 903.
(4) Wang, Y.; Herron, N. *Science* **1996**, *273*, 632.
(5) Kamat, P. V. Composite Semiconductor Nanoclusters. In *Semiconductor Nanoclusters−Physical, Chemical and Catalytic Aspects*; Kamat, P. V., Meisel, D., Eds.; Elsevier Science: Amsterdam, 1997; p 237.
(6) Nirmal, M.; Dabbousi, B. O.; Bawendi, M. G.; Macklin, J. J.; Trautman, J. K.; Harris, T. D.; Brus, L. E. *Nature* **1996**, *383*, 802.
(7) Pileni, M. P. *New J. Chem.* **1998**, 693.
(8) Henglein, A. *Langmuir* **1998**, *14*, 6738.
(9) Toshima, N.; Yonezawa, T. *New J Chem* **1998**, *22*, 1179.
(10) (a) Link, S.; El-Sayed, M. A. *J. Phys. Chem. B* **1999**, *103*, 4212. (b) El-Sayed, M. A. *Acc. Chem. Res.* **2001**, *34*, 257.
(11) Kim, S.-H.; Medeiros-Ribeiro, G.; Ohlberg, D. A. A.; Stanley Williams, R.; Heath, J. R. *J. Phys. Chem. B.* **1999**, *103*, 10341.
(12) Gomez-Romero, P. *Adv. Mater.* **2001**, *13*, 163.
(13) Dick, K.; Dhanasekaran, T.; Zhang, Z.; Meisel, D. *J. Am. Chem. Soc.* **2002**, *124*, 2312.

(14) Hickman, J. J.; Ofer, D.; Laibinis, P. E.; Whitesides, G. M.; Wrighton, M. S. *Science* **1991**, *252*, 688.
(15) Chen, S.; Ingram, R. S.; Hostetler, M. J.; Pietron, J. J.; Murray, R. W.; Schaaff, T. G.; Khoury, J. T.; Alvarez, M. M.; Whetten, R. L. *Science* **1998**, *280*, 2098.
(16) Elghanian, R.; Storhoff, J. J.; Mucic, R. C.; Letsinger, R. L.; Mirkin, C. A. *Science* **1997**, *277*, 1078.
(17) Markovich, G.; Collier, C. P.; Henrichs, S. E.; Remacle, F.; Levine, R. D.; Heath, J. R. *Acc. Chem. Res.* **1999**, *32*, 415.
(18) Willner, I.; Willner, B. *Pure Appl. Chem.* **2001**, *73*, 535.
(19) Sass, J. K.; Sen, R. K.; Meyer, E.; Gerischer, H. *Surf. Sci.* **1974**, *44*, 515.
(20) Mulvaney, P.; Linnert, T.; Henglein, A. *J. Phys. Chem.* **1991**, *95*, 7843.
(21) Linnert, T.; Mulvaney, P.; Henglein, A. *Ber. Bunsen-Ges. Phys. Chem.* **1991**, *95*, 838.
(22) Turkevich, J.; Stevenson, P. L.; Hillier, J. *Discuss. Faraday Soc.* **1951**, *11*, 55.
(23) Suslick, K. S. *Science* **1990**, *247*, 1439.
(24) Henglein, A.; Giersig, M. *J. Phys. Chem. B* **1999**, *103*, 9533.
(25) Henglein, A. *Chem. Mater.* **1998**, *10*, 444.
(26) Henglein, A.; Meisel, D. *Langmuir* **1998**, *14*, 7392.
(27) Goia, D. V.; Matijevic, E. *New J. Chem.* **1998**, *22*, 1203.
(28) Belloni, J.; Mostafavi, M.; Remita, H.; Marignier, J. L.; Delcourt, M. O. *New J. Chem.* **1998**, *22*, 1239.
(29) Treguer, M.; de Cointet, C.; Remita, H.; Khatouri, J.; Mostafavi, M.; Amblard, J.; Belloni, J.; de Keyzer, R.; Belloni, J. *J. Phys. Chem. B* **1998**, *102*, 4310.
(30) Henglein, A. *J. Phys. Chem. B* **2000**, *104*, 6683.
(31) Templeton, A. C.; Wuelfing, W. P.; Murray, R. W. *Acc. Chem. Res.* **2000**, *33*, 27.
(32) Rodríguez-Gattorno, G.; Díaz, D.; Rendón, L.; Hernández-Segura, G. O. *J. Phys. Chem. B.* **2002**, *106*, 2482.
(33) Brust, M.; Walker, M.; Bethell, D.; Schffrin, D. J.; Whyman, R. *J. Chem. Soc., Chem. Commun.* **1994**, 801.
(34) Brust, M.; Fink, J.; Bethell, D.; Schiffrin, D. J.; Kiely, C. *J. Chem. Soc., Chem. Commun.* **1995**, 1655.
(35) Kolb, U.; Quaiser, S. A.; Winter, M.; Reetz, M. T. *Chem. Mater.* **1996**, *8*, 1889.
(36) Fink, J.; Kiely, C.; Bethell, D.; Schiffrin, D. J. *Chem. Mater.* **1998**, *10*, 922.
(37) Perez, M.; Pradeau, J.-P.; Albouy, P.-A.; Perez-Omil, J. *Chem. Mater.* **1999**, *11*, 3460.
(38) Subramanian, V.; Wolf, E.; Kamat, P. V. *J. Phys. Chem. B* **2001**, *105*, 11439.
(39) Niidome, Y.; Hori, A.; Sato, T.; Yamada, S. *Chem. Lett.* **2000**, 310.
(40) George Thomas, K.; Zajicek, J.; Kamat, P. V. *Langmuir* **2002**, *18*, 3722.
(41) Chandrasekharan, N.; Kamat, P. V. *Nano Lett.* **2001**, *1*, 67.
(42) Hostetler, M. J.; Wingate, J. E.; Zhong, C.-J.; Harris, J. E.; Vachet, R. W.; Clark, M. R.; Londono, J. D.; Green, S. J.; Stokes, J. J.; Wignall, G. D.; Glish, G. L.; Porter, M. D.; Evans, N. D.; Murray, R. W. *Langmuir* **1998**, *14*, 17.
(43) Yu, Y. Y.; Chang, S. S.; Lee, C. L.; Wang, C. R. C. *J Phys Chem B* **1997**, *101*, 6661.
(44) Han, M. Y.; Quek, C. H. *Langmuir* **2000**, *16*, 362.
(45) van der Zande, B. M. I.; Böhmer, M. R.; Fokkink, L. G. J.; Schönenberger, C. *Langmuir* **2000**, *16*, 451.
(46) Jana, N. R.; Gearheart, L.; Murphy, C. J. *J. Phys. Chem. B* **2001**, *105*, 4065.
(47) Quiros, I.; Yamada, M.; Kubo, K.; Mizutani, J.; Kurihara, M.; Nishihara, H. *Langmuir* **2002**, *18*, 1413.
(48) Jin, R. C.; Cao, Y. W.; Mirkin, C. A.; Kelly, K. L.; Schatz, G. C.; Zheng, J. G. *Science* **2001**, *294*, 1901.
(49) Murakoshi, K.; Nakato, Y. *Adv. Mater.* **2000**, *12*, 791.
(50) Han, S. W.; Lee, I.; Kim, K. *Langmuir* **2002**, *18*, 182.
(51) Fujiwara, H.; Yanagida, S.; Kamat, P. V. *J. Phys. Chem. B* **1999**, *103*, 2589.
(52) Porter, L. A.; Ji, D.; Westcott, S. L.; Graupe, M.; Czernuszewicz, R. S.; Halas, N. J. *Langmuir* **1998**, *14*, 7378.
(53) Westcott, S. L.; Oldenburg, S. J.; Lee, T. R.; Halas, N. J. *Chem. Phys. Lett.* **1999**, *300*, 651.
(54) Brust, M.; Kiely, C. J.; Bethell, D.; Schiffrin, D. J. *J. Am. Chem. Soc.* **1998**, *120*, 12367.
(55) Giersig, M.; Mulvaney, P. *Langmuir* **1993**, *9*, 3408.
(56) Sarathy, K. V.; Raina, G.; Yadav, R., T.; Kulkarni, G. U.; Rao, C. N. R. *J. Phys. Chem. B* **1997**, *101*, 9876.
(57) Kiely, C. J.; Brust, M.; Bethell, D.; Schiffrin, D. J. *Nature* **1998**, *396*, 444.
(58) Badia, A.; Cuccia, L.; Demers, L.; Morin, F. G.; Lennox, R. B. *J. Am. Chem. Soc.* **2000**, *119*, 2682.
(59) Giersig, M.; Mulvaney, P. *J. Phys. Chem.* **1993**, *97*, 6334.
(60) Amihood, D.; Katz, E.; Willner, I. *Langmuir* **1995**, *11*, 1313.
(61) Green, S. J.; Stokes, J. J.; Hostetler, M. J.; Pietron, J.; Murray, R. W. *J. Phys. Chem. B* **1997**, *101*, 2663.
(62) Badia, A.; Demers, L.; Dickinson, L.; Morin, F. G.; Lennox, R. B.; Reven, L. *J. Am. Chem. Soc.* **1997**, *119*, 11104.
(63) Hostetler, M. J.; Templeton, A. C.; Murray, R. W. *Langmuir* **1998**, *15*, 3782
(64) Kohlmann, O.; Steinmetz, W. E.; Mao, X.-A.; Wuelfing, W. P.; Templeton, A. C.; Murray, R. W.; and Charles S. Johnson, J. C. S. *J. Phys. Chem. B* **2001**, *105*, 8801.
(65) Chen, M. C.; Tsai, S. D.; Chen, M. R.; Ou, S. Y.; Li, W. H.; Lee, K. C. *Phys. Rev. B* **1995**, *51*, 4507.
(66) Keating, C. D.; Kovaleski, K. K.; Natan, M. J. *J. Phys. Chem. B* **1998**, *102*, 9414.
(67) Merklin, G. T.; Griffiths, P. R. *J. Phys. Chem. B* **1997**, *101*, 5810.
(68) Bjerke, A. E.; Griffiths, P. R.; Theiss, W. *Anal. Chem.* **1999**, *71*, 1967.
(69) Wandlowski, T.; Ataka, K.; Mayer, D. *Langmuir* **2002**, *18*, 4331.
(70) Hulteen, J. C.; Treichel, D. A.; Smith, M. T.; Duval, M. L.; Jensen, T. R.; Van Duyne, R. P. *J. Phys. Chem. B* **1999**, *103*, 3854.
(71) Pignataro, B.; De Bonis, A.; G., C.; Sassi, P.; Cataliotti, R. S. *J. Chem. Phys.* **2000**, *113*, 5947.
(72) Musick, M. D.; Keating, C. D.; Lyon, L. A.; Botsko, S. L.; Pena, D. J.; Holliway, W. D.; McEvoy, T. M.; Richardson, J. N.; Natan, M. J. *Chem. Mater.* **2000**, *12*, 2869.
(73) Brown, K. R.; G., W. D.; Natan, M. J. *Chem. Mater.* **2000**, *12*, 306.
(74) Michaels, A. M.; Jiang, J.; Brus, L. *J. Phys. Chem. B* **2000**, *104*, 11965.
(75) Oldenburg, S. J.; Westcott, S. L.; Averitt, R. D.; Halas, N. J. *J. Chem. Phys.* **1999**, *111*, 4729.
(76) Mulvaney, P. Spectroscopy of metal colloids. Some comparisons with semiconductor colloids. In *Semiconductor Nanoclusters−Physical, Chemical and Catalytic Aspects*; Kamat, P. V., Meisel, D., Eds.; Elsevier Science: Amsterdam, 1997; p 99.
(77) Kreibig, U.; Vollmer, M. *Optical Properties of Metal Clusters*; Springer: Berlin, 1995.
(78) Mulvaney, P. *Langmuir* **1996**, *12*, 788.
(79) Alvarez, M. M.; Khoury, J. T.; Schaaff, T. G.; Shafigullin, M. N.; Vezmar, I.; Whetten, R. L. *J. Phys. Chem. B* **1997**, *101*, 3706.
(80) Schaaff, T. G.; Shafigullin, M. N.; Khoury, J. T.; Vezmar, I.; Whetten, R. L.; Cullen, W. G.; First, P. N.; Gutierrez-Sing, C.; Ascensio, J.; Jose-Yacaman, M. J. *J. Phys. Chem. B* **1997**, *101*, 7885.
(81) Heath, J. R.; Knobler, C. M.; Leff, D. V. *J. Phys. Chem. B* **1997**, *101*, 189.
(82) Kreibig, U.; Gartz, M.; Hilger, A.; Hovel, H. Mie-Plasmon Spectroscopy: A Tool of Surface Science. In *Fine Particles Science and Technology*; Pelizzatti, E., Ed.; Kulwer Academic Publishers: Boston, 1996; p 499.
(83) Mirkin, C. A.; Letsinger, R. L.; Mucic, R. C.; Storhoff, J. J. *Nature* **1996**, *382*, 607.
(84) Link, S.; Mohamed, M. B.; El-Sayed, M. A. *J. Phys. Chem. B* **1999**, *103*, 3073.
(85) Kittel, C. *Introduction to Solid State Physics*, 2nd ed.; Wiley: New York, 1956.
(86) Shklyarevskii, I. N.; Anachkova, E.; Blyashenko, G. S. *Opt. Spectrosc. (USSR)* **1977**, *43*, 427.
(87) Underwood, S.; Mulvaney, P. *Langmuir* **1994**, *10*, 3427.
(88) Hughes, A. E.; Jain, S. C. *Adv. Phys.* **1979**, *28*, 717.
(89) Templeton, A. C.; Pietron, J. J.; Murray, R. W.; Mulvaney, P. *J. Phys. Chem. B* **2000**, *104*, 564
(90) Lin, S. T.; Franklin, M. T.; Klabunde, K. J. *Langmuir* **1986**, *2*, 9.
(91) Furstner, A. *Active Metals: Preparation Characterization Applications*; John Wiley & Sons: New York, 1995.
(92) Pileni, M. P. *J. Phys. Chem. B* **2001**, *105*, 3358.
(93) Linnert, T.; Mulvaney, P.; Henglein, A. *J. Phys. Chem.* **1993**, *97*, 679.
(94) Gutierrez, M.; Henglein, A. *J. Phys. Chem.* **1993**, *97*, 11368.
(95) Henglein, A.; Mulvaney, P.; Linnert, T. *Faraday Discuss.* **1991**, *92*, 31.
(96) Persson, B. N. J. *Phys. Rev. B* **1989**, *39*, 8220.
(97) Wilcoxon, J. P.; Martin, J. E.; Parsapour, F.; Wiedenman, B.; Kelley, D. F. *J. Chem. Phys* **1998**, *108*, 9137.
(98) Mohamed, M. B.; Volkov, V.; Link, S.; El-Sayed, M. A. *Chem. Phys. Lett.* **2000**, *317*, 517.
(99) Huang, T.; Murray, R. W. *J. Phys. Chem. B* **2001**, *105*, 12498.
(100) Sato, T.; Ichikawa, T.; Ito, T.; Yonezawa, Y.; Kadono, K.; Sakaguchi, T.; Miya, M. *Chem. Phys. Lett.* **1995**, *242*, 310.
(101) François, L.; Mostafavi, M.; Belloni, J.; Delouis, J.-F.; Delaire, J.; Feneyrou, P. *J. Phys. Chem. B* **2000**, *104*, 6133.
(102) Lee, P. C.; Meisel, D. *J. Phys. Chem.* **1982**, *86*, 3391.
(103) Freeman, R. G.; Hommer, M. B.; Grabar, K. C.; Jackson, M. A.; Natan, M. J. *J. Phys. Chem.* **1996**, *100*, 718.

(104) Oldenburg, S. J.; Westcott, S. L.; Averitt, R. D.; Halas, N. J. *J. Chem. Phys.* **1999**, *111*, 4729.
(105) Zhang, J. Z. *Acc. Chem. Res.* **1997**, *30*, 423.
(106) Link, S.; El-Sayed, M. A. *J. Phys. Chem. B* **1999**, *103*, 8410.
(107) Hodak, J.; Henglein, A.; Hartland, G. V. *J. Phys. Chem. B* **2000**, *104*, 9954.
(108) Heilweil, E. J.; Hochstrasser, R. M. *J. Chem. Phys.* **1985**, *82*, 179.
(109) Aktsipetrov, O. A.; Elyutin, P. V.; Fedyanin, A. A.; Nikulin, A. A.; Rubtsov, A. N. *Surf. Sci.* **1995**, *325*, 343.
(110) Mie, G. *Ann. Phys. B* **1908**, *25*, 377.
(111) Ahmadi, T. S.; Logunov, S. L.; El-Sayed, M. A. *J. Phys. Chem.* **1996**, *100*, 8053.
(112) Hodak, J.; Martini, I.; Hartland, G. V. *Chem. Phys. Lett.* **1998**, *284*, 135.
(113) Kamat, P. V.; Flumiani, M.; Hartland, G. *J. Phys. Chem. B* **1998**, *102*, 3123.
(114) Hodak, J.; Henglein, A.; Giersig, M.; Hartland, G. V. *J. Phys. Chem. B* **2000**, *104*, 11708.
(115) Link, S.; Wang, Z. L.; El-Sayed, M. A. *J. Phys. Chem. B* **1999**, *103*, 3529.
(116) Kamat, P. V.; Flumiani, M.; Dawson, A. *Colloids Surf., A* **2002**, *202*, 269.
(117) Takami, A.; Yamada, H.; Nakano, K.; Koda, S. *Jpn. J. Appl. Phys.* **1996**, *35*, L781.
(118) Link, S.; Burda, C.; Mohamed, M. B.; Nikoobakht, B.; El-Sayed, M. A. *J. Phys. Chem. A* **1999**, *103*, 1165.
(119) Link, S.; Wang, Z. L.; El-Sayed, M. A. *J. Phys. Chem. B* **2000**, *104*, 6767.
(120) Dawson, A.; Kamat, P. V. *J. Phys. Chem. B* **2001**, *105*, 960.
(121) Murakoshi, K.; Tanaka, H.; Sawai, Y.; Nakato, Y. *J. Phys. Chem. B* **2002**, *106*, 3041.
(122) Link, S.; Burda, C.; Nikoobakht, B.; El-Sayed, M. A. *J. Phys. Chem. B* **2000**, *104*, 6152.
(123) Link, S.; El-Sayed, M. A. *J Chem Phys* **2001**, *114*, 2362.
(124) Chandrasekharan, N.; Kamat, P. V.; Hu, J.; Jones, G., II *J. Phys. Chem. B* **2000**, *104*, 11103.
(125) Takami, A.; Kurita, H.; Koda, S. *J. Phys. Chem. B* **1999**, *103*, 1226.
(126) Logunov, S. L.; Ahmadi, T. S.; El-Sayed, M. A.; Khoury, J. T.; Whetten, R. L. *J. Phys. Chem. B* **1997**, *101*, 3713.
(127) Shanghavi, B.; Kamat, P. V. *J. Phys. Chem. B* **1997**, *101*, 7675.
(128) Link, S.; Burda, C.; Nikoobakht, B.; El-Sayed, M. A. *Chem. Phys. Lett.* **1999**, *315*, 12.
(129) Mohamed, M. B.; Ismail, K. Z.; Link, S.; El-Sayed, M. A. *J. Phys. Chem. B* **1998**, *102*, 9370.
(130) Zhao, X. M.; Xia, Y. N.; Whitesides, G. M. *J. Mater. Chem.* **1997**, *7*, 1069.
(131) Whetten, R. L.; Shafigullin, M. N.; Khoury, J. T.; Schaaff, T. G.; Vezmar, I.; Alvarez, M. M.; A. W. *Acc. Chem. Res.* **1999**, *32*, 397.
(132) McConnell, W. P.; Novak, J. P.; Brousseau, L. C., III; Fuierer, R. R.; Tenent, R. C.; Feldheim, D. L. *J. Phys. Chem. B* **2000**, *104*, 8925.
(133) Shipway, A. N.; Katz, E.; Willner, I. *Phys. Chem. Phys* **2000**, *1*, 18.
(134) Templeton, A. C.; Cliffel, D. E.; Murray, R. W. *J. Am. Chem. Soc.* **1999**, *121*, 7081.
(135) Fitzmaurice, D.; Rao, S. N.; Preece, J. A.; Stoddart, J. F.; Wenger, S.; Zaccheroni, N. *Angew. Chem., Int. Ed. Engl.* **1999**, *38*, 1147.
(136) Han, W.; Li, S.; Lindsay, S. M.; Gust, D.; Moore, T. A.; Moore, A. L. *Langmuir* **1996**, *12*, 5742.
(137) Jana, N. R.; Pal, T.; Sau, T. K. *Rad. Phys. Chem.* **1997**, *49*, 127.
(138) Makarova, O. V.; Ostafin, A. E.; Miyoshi, H.; Norris, J. R.; Meisel, D. *J. Phys. Chem. B* **1999**, *103*, 9080.
(139) Hainfeld, J. F.; Furuya, F. R. *J. Histochem. Cytochem.* **1992**, *40*, 177.
(140) Ribrioux, S.; Kleymann, G.; Haase, W.; Heitmann, K.; Ostermeier, C.; Michel, H. *J. Histochem. Cytochem.* **1996**, *44*, 207.
(141) Powell, R. D.; Halsey, C. M. R.; Hainfeld, J. F. *Microscopy Research and Technique* **1998**, *42*, 2.
(142) Hayward, R. C.; Saville, D. A.; Aksay, I. A. *Nature* **2000**, *404*, 56.
(143) Bauer, G.; Pittner, F.; Schalkhammer, T. *Mikrochim. Acta* **1999**, *131*, 107.
(144) Aherne, D.; Nagaraja Rao, S.; Fitzmaurice, D. *J. Phys. Chem. B* **1999**, *103*, 1821.
(145) Hu, J.; Zhang, J.; Liu, F.; Kittredge, K.; Whitesell, J. K.; Fox, M. A. *J. Am. Chem. Soc.* **2001**, *123*, 1464.
(146) Brust, M.; Bethell, D.; Kiely, C. J.; Schiffrin, D. J. *Langmuir* **1998**, *14*, 5425.
(147) Ishida, A.; Sakata, Y.; Majima, T. *J. Chem. Soc., Chem. Comm* **1998**, 57.
(148) Novak, J. P.; Brousseau, L. C.; Vance, F. W.; Johnson, R. C.; Lemon, B. I.; Hupp, J. T.; Feldheim, D. L. *J. Am. Chem. Soc.* **2000**, *122*, 12029.
(149) Walter, D. G.; Campbell, D. J.; Mirkin, C. A. *J. Phys. Chem. B* **1999**, *103*, 402.
(150) Henrichs, S. E.; Sample, J. L.; Shiang, J. J.; Heath, J. R.; Collier, C. P.; Saykally, R. J. *J. Phys. Chem. B* **1999**, *103*, 3524.
(151) Jensen, T. R.; Malinsky, M. D.; Haynes, C. L.; Van Duyne, R. P. *J. Phys. Chem. B* **2000**, *104*, 10549.
(152) Piner, R. D.; Zhu, J.; Xu, F.; Hong, S. H.; Mirkin, C. A. *Science* **1999**, *283*, 661.
(153) Haynes, C. L.; Van Duyne, R. P. *J. Phys. Chem. B* **2001**, *105*, 5599.
(154) Ivanisevic, A.; Mirkin, C. A. *J. Am. Chem. Soc.* **2001**, *123*, 7887.
(155) Valina-Saba, M.; Bauer, G.; Stich, N.; Pittner, F.; Schalkhammer, T. *Mater. Sci. Eng., C* **1999**, *8*−*9*, 205.
(156) Gobi, K. V.; Mizutani, F. *J. Electroanal. Chem.* **2000**, *484*, 172.
(157) Willner, I.; Pardo-Yissar, V.; Katz, E.; Ranjit, K. T. *J. Electroanal. Chem.* **2001**, *497*, 172.
(158) Reynolds, R. A.; Mirkin, C. A.; Letsinger, R. L. *Pure Appl. Chem.* **2000**, *72*, 229.
(159) Demers, L. M.; Mirkin, C. A.; Mucic, R. C.; Reynolds, R. A.; Letsinger, R. L.; Elghanian, R.; Viswanadham, G. *Anal. Chem.* **2000**, *72*, 5535.
(160) Brust, M.; Blass, P. M.; Bard, A. J. *Langmuir* **1997**, *13*, 5602.
(161) Lahav, M.; Gabriel, T.; Shipway, A. N.; Willner, I. *J. Am. Chem. Soc.* **1999**, *121*, 258.
(162) Lahav, M.; Katz, E.; Doron, A.; Patolsky, F.; Willner, I. *J. Am. Chem. Soc.* **1999**, *121*, 862.
(163) Imahori, H.; Arimura, M.; Hanada, T.; Nishimura, Y.; Yamazaki, I.; Sakata, Y.; Fukuzumi, S. *J. Am. Chem. Soc.* **2000**, *122*, 335.
(164) Imahori, H.; Norieda, H.; Yamada, H.; Nishimura, Y.; Yamazaki, I.; Sakata, Y.; Fukuzumi, S. *J. Am. Chem. Soc.* **2001**, *123*, 100.
(165) Henglein, A.; Meisel, D. *J. Phys. Chem. B* **1998**, *102*, 8364.
(166) Benesi, H. A.; Hildebrand, J. H. *J. Am. Chem. Soc.* **1949**, *71*, 2703.
(167) Liu, D.; Kamat, P. V. *J. Electrochem. Soc.* **1995**, *142*, 835.
(168) Nasr, C.; Liu, D.; Hotchandani, S.; Kamat, P. V. *J. Phys. Chem.* **1996**, *100*, 11054.
(169) Sayama, K.; Sugino, M.; Sugihara, H.; Abe, Y.; Arakawa, H. *Chem. Lett.* **1998**, 753.
(170) Ikegami, K.; Mingotaud, C.; Lan, M. *J. Phys. Chem. B* **1999**, *103*, 11261.
(171) Saito, K. *J. Phys. Chem. B* **1999**, *103*, 6579.
(172) Pagnot, T.; Barchiesi, D.; Tribillon, G. *Appl. Phys. Lett.* **1999**, *75*, 4207.
(173) Kerker, M. *J. Colloid Interface Sci.* **1985**, *105*, 297.
(174) Stenzel, O.; Stendal, A.; Voigtsberger, A.; C., V. B. *Sol. Energy Mater. Sol. Cells* **1995**, *37*, 337.
(175) George Thomas, K.; Kamat, P. V. *J. Am. Chem. Soc.* **2000**, *122*, 2655
(176) Gust, D.; Moore, T. A.; Moore, A. L. *Acc. Chem. Res.* **1993**, *26*, 198.
(177) Kamat, P. V.; Barazzouk, S.; Hotchandani, S.; George Thomas, K. *Chem., Eur. J.* **2000**, *6*, 3914.
(178) Creager, S. E.; Collard, D. M.; Fox, M. A. *Langmuir* **1990**, *6*, 1617.
(179) Akiyama, T.; Imahori, H.; Ajawakom, A.; Sakata, Y. *Chem. Lett.* **1996**, 907.
(180) Imahori, H.; Azuma, T.; Ajavakom, A.; Norieda, H.; Yamada, H.; Sakata, Y. *J. Phys. Chem. B* **1999**, *103*, 7233.
(181) Arias, F.; Godinez, L. A.; Wilson, S. R.; Kaifer, A. E.; Echegoyen, L. *J. Am. Chem. Soc.* **1996**, *118*, 6086.
(182) Badia, A.; Singh, S.; Demers, L.; Cuccia, L.; Brown, G. R.; Lennox, R. B. *Chem., Euro. J.* **1996**, *2*, 359.
(183) Johnson, S. R.; Evans, S. D.; Mahon, S. W.; Ulman, A. *Langmuir* **1997**, *13*, 51.
(184) Enger, O.; Nuesch, F.; Fibbioli, M.; Echegoyen, L.; Pretsch, E.; Diederich, F. *J. Mater. Chem.* **2000**, *10*, 2231.
(185) Terasaki, N.; Akiyama, T.; Yamada, S. *Chem. Lett.* **2000**, 668.
(186) Avouris, P.; Persson, B. N. J. *J. Phys. Chem.* **1984**, *88*, 837.
(187) Fujihara, H.; Nakai, H. *Langmuir* **2001**, *17*, 6393.
(188) Sudeep, P. K.; Ipe, B. I.; George Thomas, K.; George, M. V.; Barazzouk, S.; Hotchandani, S.; Kamat, P. V. *Nano Lett.* **2002**, *2*, 29.
(189) George Thomas, K.; Biju, V.; George, M. V.; Guldi, D. M.; Kamat, P. V. *J. Phys. Chem. B* **1999**, *103*, 8864.
(190) Biju, V.; Barazzouk, S.; George Thomas, K.; George, M. V.; Kamat, P. V. *Langmuir* **2001**, *17*, 2930.
(191) Ipe, B. I.; George Thomas, K.; Barazzouk, S.; Hotchandani, S.; Kamat, P. V. *J. Phys. Chem. B* **2002**, *106*, 18.
(192) Thomas, J. K. *J. Phys. Chem.* **1987**, *91*, 267.
(193) Hicks, J. F.; Templeton, A. C.; Chen, S.; Sheran, K. M.; Jasti, R.; Murray, R. W.; Debord, J.; Schaaff, T. G.; Whetten, R. L. *Anal. Chem.* **1999**, *71*, 3703.
(194) Chen, S.; Murray, R. W. *J. Phys. Chem. B* **1999**, *103*, 9996.

(195) Li, J.; Yamada, Y.; Murakoshi, K.; Nakatoa, Y. *Chem. Commun.* **2001**, 2170.
(196) Henglein, A.; Lindig, B.; Westerhausen, J. *J. Phys. Chem.* **1981**, *85*, 1627.
(197) Reese, R. S.; Fox, M. A. *Canad. J. Chem.* **1999**, *77*, 1077.
(198) Chen, M. M. Y.; Katz, A. *Langmuir* **2002**, *18*, 2413.
(199) Wang, T. X.; Zhang, D. Q.; Xu, W.; Yang, J. L.; Han, R.; Zhu, D. B. *Langmuir* **2002**, *18*, 1840.
(200) Czarnick, A. N. In *Fluorescent Chemosensors for Ion and Molecular Recognition*; Czarnik, A. N., Ed.; American Chemical Society: Washington, DC, 1992; p 104.
(201) Czarnick, A. N. *Acc. Chem. Res.* **1994**, *27*, 302.
(202) Bissel, R. A.; de Silva, A. P.; Gunaratne, H. Q. N.; Lynch, P. L. M.; Maguire, G. E. M.; Sandanayake, K. R. A. S. *Chem. Soc. Rev.* **1992**, *21*, 187.
(203) de Silva, A. P.; Gunaratne, H. Q. N.; Gunnlaugsson, T.; Huxley, A., J. M.; McRoy, C. P.; Rademacher, J. T.; Rice, T. E. *Chem. Rev.* **1997**, *97*, 1515.
(204) Kamat, P. V.; Barazzouk, S.; Hotchandani, S. *Angew. Chem., Int. Ed.* **2002**. In press.
(205) Kamat, P. V. *Chem. Rev.* **1993**, *93*, 267.
(206) Bard, A. J. *J. Phys. Chem.* **1982**, *86*, 172.
(207) Bard, A. J.; Fox, M. A. *Acc. Chem. Res.* **1995**, *28*, 141.
(208) Nosaka, Y.; Norimatsu, K.; Miyama, H. *Chem. Phys. Lett.* **1984**, *106*, 128.
(209) Nasr, C.; Hotchandani, S.; Kim, W. Y.; Schmehl, R. H.; Kamat, P. V. *J. Phys. Chem. B* **1997**, *101*, 7480.
(210) Nasr, C.; Hotchandani, S.; Kamat, P. V. *J. Phys. Chem. B* **1998**, *102*, 10047.
(211) Vinodgopal, K.; Kamat, P. V. *Environ. Sci. Technol.* **1995**, *29*, 841.
(212) Tada, H.; Teranishi, T. K.; Yo-ichi, I.; Ito, S. *Langmuir* **2000**, *16*, 3304.
(213) Pastoriza-Santos, I.; Koktysh, D. S.; Mamedov, A. A.; Giersig, M.; Kotov, N. A.; Liz-Marzán, L. M. *Langmuir* **2000**, *16*, 2731.
(214) de Tacconi, N. R.; Carmona, J.; Rajeshwar, K. *J. Phys. Chem. B* **1997**, *101*, 10151.
(215) Chen, S. H.; Kimura, K. *Chem. Lett.* **1999**, 233.
(216) Vijaya Sarathy, K.; John Thomas, P.; Kulkarni, G. U.; Rao, C. N. R. *J. Phys. Chem. B* **1999**, *103*, 399.
(217) Bakkers, E. P. A. M.; Reitsma, E.; Kelly, J. J.; Vanmaekelbergh, D. *J. Phys. Chem. B* **1999**, *103*, 2781.
(218) Averitt, R. D.; Westcott, S. L.; Halas, N. J. *J. Opt. Soc. Am. B. Opt. Phys.* **1999**, *16*, 1814.
(219) Averitt, R. D.; Westcott, S. L.; Halas, N. J. *J. Opt. Soc. Am. B.* **1999**, *16*, 1824.
(220) Oldenburg, S. J.; Jackson, J. B.; Westcott, S. L.; Halas, N. J. *Appl. Phys. Lett.* **1999**, *75*, 2897.
(221) Wood, A.; Giersig, M.; Mulvaney, P. *J. Phys. Chem. B* **2001**, *105*, 8810.
(222) Kamat, P. V. *Langmuir* **1985**, *1*, 608.
(223) Behar, D.; Bevan, P. L. T.; Scholes, G. *J. Phys. Chem.* **1972**, *76*, 1537.
(224) Dawson, A.; Kamat, P. V. *J. Phys. Chem. B* **2000**, *104*, 11842.
(225) Kraeutler, B.; Bard, A. J. *J. Am. Chem. Soc.* **1978**, *100*, 4317.
(226) Yesodharan, E.; Graetzel, M. *Helv. Chim. Acta* **1983**, *66*, 2145.
(227) Baltzer, P.; Davidson, R. S.; Tseung, A. C.; Graetzel, M.; Kiwi, J. *J. Am. Chem. Soc.* **1984**, *106*, 1504.
(228) Borgarello, E.; Harris, R.; Serpone, N. *Nouv. J. Chim.* **1985**, *9*, 743.
(229) Amouyal, E.; Koffi, P. *J. Photochem.* **1985**, *29*, 227.
(230) Mills, A.; Williams, G. *J. Chem. Soc., Faraday Trans. 1* **1989**, *85*, 503.
(231) Ashokkumar, M. *Int. J. Hydrogen Energy* **1998**, *23*, 427.
(232) Chandrasekharan, N.; Kamat, P. V. *J. Phys. Chem. B* **2000**, *104*, 10851.
(233) Meier, A.; Uhlendorf, I.; Meissner, D. *Electrochim. Acta* **1995**, *40*, 1523.
(234) Hinogami, R.; Nakamura, Y.; Yae, S.; Nakato, Y. *J. Phys. Chem. B* **1998**, *102*, 974.
(235) Hiesgen, R.; Meissner, D. *J. Phys. Chem. B* **1998**, *102*, 6549.
(236) Bethell, D.; Brust, M.; Schiffrin, D. J.; Kiely, C. *J. Electroanal. Chem.* **1996**, *409*, 137.
(237) Carmichael, I.; Hug, G. L. *J. Phys. Chem. Ref. Data* **1986**, *15*.